Hadronic CP Violation in the 2HDM

Wolfgang Altmannshofer*[a], Joachim Brod†[b], Patipan Uttayarat‡[c], Daniil Volkov§[b]

[a] *Department of Physics and Santa Cruz Institute for Particle Physics, University of California, Santa Cruz, CA 95064, USA*

[b] *Department of Physics, University of Cincinnati, Cincinnati, OH 45221, USA*

[c] *Department of Physics, Srinakharinwirot University, 114 Sukhumvit 23rd Rd., Wattana, Bangkok 10110, Thailand*

November 13, 2025

Abstract

We present the first complete two-loop calculation of the electric and chromo-electric dipole moments of the light quarks and the gluon, as well as contributions to CP-violating lepton-quark interactions, in the unconstrained two-Higgs doublet model. We include the most general Yukawa interactions of the Higgs doublets with the Standard Model fermions up to quadratic order, and allow for generic phases in the Higgs potential. We pay particular attention to a consistent treatment of all fermionic contributions in the low-energy effective theory, including a consistent renormalization-group summation of all leading-logarithmic effects. This latter part of the work is independent of the specific UV model and can generally be applied to a large class of models that do not introduce new light degrees of freedom. A `python` implementation of our results is provided via a public git repository.

1 Introduction

Bounds on electric dipole moments (EDMs) provide stringent constraints on CP-violating phases that are crucial for models of electroweak baryogenesis [1]. In the two-Higgs doublet model (2HDM) [2], the desired CP violation is supplied by the complex phases associated with the Higgs sector that is extended with respect to the SM by adding a second Higgs doublet. It is mainly the phases in the Yukawa couplings to the third fermion generation that play a role in models of electroweak baryogenesis [3–10]. The Higgs potential of the 2HDM allows for a first-order phase transition for an appropriate choice of parameters [11–23].

*`waltmann@ucsc.edu`

†`joachim.brod@uc.edu`

‡`patipan@g.swu.ac.th`

§`volkovdi@mail.uc.edu`

The main constraints on the CP phases arise from the non-observation of electric dipole moments (EDMs) of elementary systems such as the electron, the neutron, or atomic and molecular systems [24–27]. If one allows for the presence of phases in all the Yukawa couplings, however, it is easy to arrange for the bounds from any individual EDM to disappear due to the cancellation of the various contributions. It is therefore imperative to include as many observables as possible when testing the CP phases of the 2HDM. In Ref. [28] we have calculated the leading contributions to the electron EDM, and lepton-number violating radiative lepton decays; see also Ref. [29] for related work. Here, we focus on the EDMs of hadronic systems. In particular, we calculate the leading contributions to the light-quark (up, down, and strange) EDMs and chromo-EDMs, to the Weinberg operator (the gluon chromo-EDM), and CP-violating electron-quark interactions. These CP-violation quark and gluon interactions are not directly observable, but they induce a large variety of observable EDMs in elementary, atomic, and molecular systems; see Ref. [24] for a review.

We match the 2HDM directly to an effective theory valid below the electroweak scale, so that our results are valid for arbitrary Higgs masses (as long as they are at or above the electroweak scale). We then sum all leading large logarithms to all orders in the strong coupling constant by calculating the QCD renormalization-group (RG) evolution of the Wilson coefficients from the electroweak scale to the hadronic scale of 2 GeV. In fact, this RG evolution applies also to extensions of the SM other than the 2HDM, as long as no new degrees of freedom below the weak scale are introduced. Hence, this part of our results should be useful beyond the scope of the current analysis.

This work is structured as follows. We briefly introduce the 2HDM and establish our conventions in Sec. 2. The effective theories below the weak scale, as well as the anomalous dimensions required for the RG evolution, are introduced in Sec. 3. Our main results are contained in Sec. 4, where we provide explicit expressions for all matching conditions the weak scale. Sec. 4.2 contains a detailed discussion of the summation of large logarithms that arise from small SM fermion masses. Sec. 5 comprises a brief summary and a link to a public git repository containing a `python` implementation of our results. Finally, in App. A we collect some Fierz identities that were used in obtaining our results, and in App. B we give the gauge-dependent parts of the loop functions for some subsets of Feynman diagrams (as discussed below, all gauge dependence cancels when summing the contributions of all diagrams).

2 The 2HDM

To begin, we briefly review the general two-Higgs doublet model. This serves mainly to establish our notation and conventions; a detailed discussion can be found in Refs. [30–33]. We will work with the unconstrained 2HDM in which the SM scalar sector is extended by an additional scalar doublet, such that the scalar potential depends on two $SU(2)_L$ doublets H_1 and H_2, both with hypercharge $+1/2$. Here, we work in the the so-called Higgs basis, where only the field H_1 receives a vacuum expectation value. In that basis, the scalar potential is given by

$$\begin{aligned}\mathcal{V}(H_1,\, H_2) = {} & Y_1 H_1^\dagger H_1 + Y_2 H_2^\dagger H_2 + \Big(Y_3 H_1^\dagger H_2 + \text{c.c.}\Big) \\ & + \tfrac{1}{2} Z_1 \big(H_1^\dagger H_1\big)^2 + \tfrac{1}{2} Z_2 \big(H_2^\dagger H_2\big)^2 + Z_3 \big(H_1^\dagger H_1\big)\big(H_2^\dagger H_2\big) + Z_4 \big(H_1^\dagger H_2\big)\big(H_2^\dagger H_1\big) \\ & + \Big(\tfrac{1}{2} Z_5 \big(H_1^\dagger H_2\big)^2 + \big(Z_6\, H_1^\dagger H_1 + Z_7\, H_2^\dagger H_2\big)\big(H_1^\dagger H_2\big) + \text{c.c.}\Big)\,,\end{aligned} \tag{1}$$

where the parameters Y_1, Y_2, $Z_1, \ldots, Z_4$ are real, while Y_3 and Z_5, Z_6, Z_7 may be complex. In the Higgs basis, the components of the scalar fields can be written as

$$H_1 = \begin{pmatrix} G^+ \\ \frac{1}{\sqrt{2}}\left(v + \varphi_1^0 + iG^0\right) \end{pmatrix}, \qquad H_2 = \begin{pmatrix} H^+ \\ \frac{1}{\sqrt{2}}\left(\varphi_2^0 + ia^0\right) \end{pmatrix}, \tag{2}$$

where $v^2 = (246.2\,\mathrm{GeV})^2$. The unphysical "would-be" Goldstone boson fields are denoted by G^+ and G^0. The physical charged Higgs bosons $H^\pm$ have a squared mass given by

$$M_{H^\pm}^2 = Y_2 + \frac{1}{2} Z_3 v^2 \,. \tag{3}$$

In the presence of CP-violation, all three neutral Higgs bosons φ_1^0, φ_2^0, and a^0 mix. The corresponding symmetric squared-mass matrix $\mathcal{M}^2$ is given by

$$\frac{\mathcal{M}^2}{v^2} = \begin{pmatrix} Z_1 & \mathrm{Re}(Z_6) & -\mathrm{Im}(Z_6) \\ \mathrm{Re}(Z_6) & Y_2/v^2 + \frac{1}{2} Z_{345}^+ & -\frac{1}{2}\mathrm{Im}(Z_5) \\ -\mathrm{Im}(Z_6) & -\frac{1}{2}\mathrm{Im}(Z_5) & Y_2/v^2 + \frac{1}{2} Z_{345}^- \end{pmatrix}, \tag{4}$$

where $Z_{345}^\pm = Z_3 + Z_4 \pm \mathrm{Re}(Z_5)$. This mass matrix is diagonalized by a special orthogonal transformation that can be parameterized as

$$\begin{pmatrix} h_1 \\ h_2 \\ h_3 \end{pmatrix} = \begin{pmatrix} q_{11} & \mathrm{Re}(q_{12}) & \mathrm{Im}(q_{12}) \\ q_{21} & \mathrm{Re}(q_{22}) & \mathrm{Im}(q_{22}) \\ q_{31} & \mathrm{Re}(q_{32}) & \mathrm{Im}(q_{32}) \end{pmatrix} \begin{pmatrix} \varphi_1^0 \\ \varphi_2^0 \\ a^0 \end{pmatrix}. \tag{5}$$

We denote the masses of the three neutral mass-eigenstate Higgs bosons h_k by M_{h_k}, for $k = 1, 2, 3$. The elements of the rotation matrix in Eq. (5) can be parameterized by three angles

$$\begin{pmatrix} q_{11} & \mathrm{Re}(q_{12}) & \mathrm{Im}(q_{12}) \\ q_{21} & \mathrm{Re}(q_{22}) & \mathrm{Im}(q_{22}) \\ q_{31} & \mathrm{Re}(q_{32}) & \mathrm{Im}(q_{32}) \end{pmatrix} = \begin{pmatrix} c_{12}c_{13} & -s_{12}c_{23} - c_{12}s_{13}s_{23} & s_{12}s_{23} - c_{12}s_{13}c_{23} \\ s_{12}c_{13} & c_{12}c_{23} - s_{12}s_{13}s_{23} & -c_{12}s_{23} - s_{12}s_{13}c_{23} \\ s_{13} & c_{13}s_{23} & c_{13}c_{23} \end{pmatrix}, \tag{6}$$

where s_{ij} (c_{ij}) is $\sin\theta_{ij}$ ($\cos\theta_{ij}$). This parameterization is used in the `python` code (see Sec. 5), such that the orthogonality of the rotation matrix is manifest and no spurious entries remain.

The Yukawa interactions in the mass-eigenstate basis for the Higgs bosons and the fermions are given by [28] (see also Ref. [32])

$$\begin{aligned} \mathcal{L}_{\mathrm{Yuk}} \supset -\sum_k \sum_{ij} h_k \Bigg[&\bar{u}_{L,i} \left(\frac{m_{u_i}}{v} \delta_{ij} q_{k1} + \rho_{u,ij} q_{k2}^* \right) u_{R,j} \\ &+ \sum_{f=d,e} \bar{f}_{L,i} \left(\frac{m_{f_i}}{v} \delta_{ij} q_{k1} + \rho_{f,ij}^\dagger q_{k2} \right) f_{R,j} \Bigg] + \text{c.c.} \\ &- \sqrt{2} H^+ \left[\bar{u}_{L,i} \left(V \rho_d^\dagger \right)_{ij} d_{R,j} - \bar{u}_{R,i} \left(\rho_u^\dagger V \right)_{ij} d_{L,j} \right] - \sqrt{2} H^+ \bar{\nu}_{L,i} \rho_{\ell,ij}^\dagger e_{R,j} + \text{c.c.}\,, \end{aligned} \tag{7}$$

Here, d_L, u_L, and e_L (d_R, u_R, and e_R) denote the left-(right-)handed up-quark, down-quark, and charged lepton fields, respectively. The left-handed neutrinos are denoted with ν_L. We do not display the interactions of the unphysical Goldstone bosons, but they were included in our calculations to obtain gauge-independent results. The 3×3 matrices ρ_f contain general complex entries that comprise flavor and CP violation. The charged Higgs interactions with quarks contain the Cabibbo-Kobayashi-Maskawa (CKM) quark mixing matrix V.

In practice, we performed all calculations using the background field gauge method in the electroweak sector [34], since this leads to a drastic reduction in the complexity of the calculation. In the unbroken phase, we split all gauge fields into quantum fields and background fields (the latter denoted by a hat). We also perform a similar splitting for the field H_1 in the Higgs basis, i.e. we have

$$\hat{H}_1 = \begin{pmatrix} \hat{G}^+ \\ \frac{1}{\sqrt{2}}\big(v + \hat{\phi}_1^0 + i\hat{G}^0\big) \end{pmatrix} , \qquad H_1 = \begin{pmatrix} G^+ \\ \frac{1}{\sqrt{2}}\big(\phi_1^0 + iG^0\big) \end{pmatrix} . \tag{8}$$

We then add the following gauge-fixing term to the Lagrangian,

$$\begin{aligned} \mathcal{L}_{\rm gf} = &-\frac{1}{2\xi}\Big[\big(\delta^{ac}\partial_\mu + g_2\epsilon^{abc}\hat{W}^b_\mu\big)W^{c,\mu} - ig_2\xi\frac{1}{2}\big(\hat{H}^\dagger_{1,i}\sigma^a_{ij}H_{1,j} - H^\dagger_{1,i}\sigma^a_{ij}\hat{H}_{1,j}\big)\Big]^2 \\ &-\frac{1}{2\xi}\Big[\partial_\mu B^\mu + ig_1\xi\frac{1}{2}\big(\hat{H}^\dagger_{1,i}H_{1,i} - H^\dagger_{1,i}\hat{H}_{1,i}\big)\Big]^2 . \end{aligned} \tag{9}$$

Here, g_1 and g_2 are the gauge couplings associated with the hypercharge $U(1)_Y$ gauge boson B_μ and the triplet of weak $SU(2)_L$ gauge bosons W^a_μ, respectively, and ξ is an arbitrary gauge parameter, chosen to be the same for all weak gauge bosons, to avoid tree-level mixing between the photon and the Z boson (see Ref. [34] for details). Moreover, $s_w \equiv \sin\theta_w$ denotes the sine of the weak mixing angle, and $c_w \equiv \cos\theta_w$. The Feynman rules are obtained by expressing all fields in the broken phase and rotating to mass eigenstates. The ghost Lagrangian is constructed in the usual way [34]. For our calculation, only the Feynman rules with a single background photon field are needed. In our conventions, $\hat{A}^\mu = c_w\hat{B}^\mu - s_w\hat{W}^{3,\mu}$.

3 Renormalization-group analysis

Our goal in this work is to calculate the leading contributions to the coefficients of the low-energy effective Lagrangian, given in Eq. (32) below, that contributes to hadronic, atomic, and molecular EDMs. This low-energy Lagrangian is defined at a renormalization scale of $\mu \sim 2\,\text{GeV}$, and comprises the up-, down-, and strange-quark EDM and chromo-EDM operators, CP-odd semileptonic operators, as well as the Weinberg three-gluon operator. We restrict ourselves to flavor diagonal dipole operators, but we do include flavor off-diagonal couplings in the 2HDM. The hadronic matrix elements and contributions to observables are discussed in several reviews, see, e.g., Refs. [24, 35].

We do not assume that the Higgs bosons have masses far above the weak scale. We will therefore match the full 2HDM onto an effective five-flavor Lagrangian at the weak scale, and our results are valid for any Higgs masses at or above the weak scale.[1]

It is important to note that QCD effects are large for all hadronic EDMs [39–45], and a realistic estimate requires the systematic summation, using RG-improved perturbation theory,

[1]For Higgs-boson masses that are very much heavier than the weak scale one could alternatively match to an intermediate effective theory (EFT), such as SMEFT [36, 37] or HEFT [38], and sum the corresponding large logarithms of ratios of weak-scale and Higgs masses. This is not expected to lead to large corrections. Note, also, that all contributions to CP-odd observables are suppressed by an inverse quadratic power of the (large) Higgs masses.

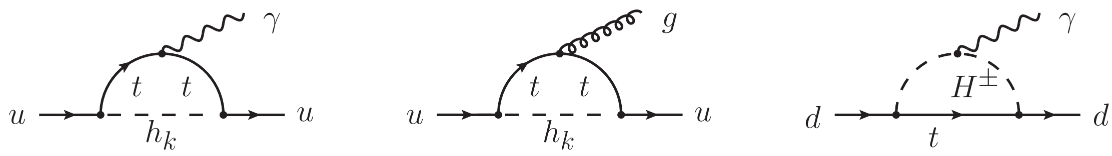

Figure 1: Representative Feynman diagrams for the one-loop contributions to the EDM (left panel) and chromo-EDM (center panel) of the up quark, and to the EDM of the down quark (right panel). Solid lines denote quarks, and dashed lines denote Higgs bosons (labelled by h_k and $H^{\pm}$).

of all large logarithms of ratios of weak-scale masses and the hadronic scale of 2 GeV. The details of the RG evolution depend on the fermion masses appearing in the diagrams. Accordingly, the matching conditions at the weak scale will need to be evaluated at tree-level, at one-loop, and at two-loop, depending on which combination of masses and couplings of the involved fermions give the numerically leading contributions. As a guide to our calculation, we now discuss the different cases.

First, we point out that all leading flavor-diagonal contributions to CP-odd observables must involve the exchange of virtual Higgs bosons. Without the additional phases in the Higgs and Yukawa sectors, contributions to electric dipole moments arise from either the QCD θ term, or the phase of the CKM matrix. Here, we work under the assumption that the θ term is negligibly small. The effect of the CKM phase on hadronic and leptonic EDM is strongly suppressed by the associated flavor violation (see Refs. [46–48] for recent estimates).

The leading contributions to the quark EDMs and CEDMs then start at one-loop order, via the exchange of virtual charged or neutral Higgs bosons (see Fig. 1). If any of the fermions in these one-loop diagrams have masses below the weak scale, the result will be dominated by the logarithm of the large ratio of fermion to Higgs mass. In this case, we use the RG to calculate the coefficient of this logarithm via the mixing of an appropriate four-fermion operator into the dipole, hence only the tree-level initial condition of that four-fermion operator needs to be calculated. Neglecting the non-logarithmic part of the diagram results in a much smaller error than neglecting the higher-order QCD corrections. If, on the other hand, all particles in the one-loop dipole diagram are heavy (masses of the order of the weak scale), the logarithm is small and the full result of the diagram is needed to calculate the initial condition. This is the case only for the down-quark dipoles with an internal charged Higgs and top quark, and for the up-quark dipoles with neutral Higgs bosons that have flavor-violating couplings to top quarks.

It has been pointed out long ago by Weinberg [49] and Dicus [50], and by Barr and Zee [51] that, if there is a large hierarchy between the Yukawa couplings, the numerically leading contribution to the dipole operators might in fact arise from two-loop diagrams. Moreover, the contributions to the gluon chromo-EDM (the "Weinberg operator" [49]) always start at two-loop order (see Fig. 8 below). To be fully general, we do not assume any hierarchy between the Yukawa couplings (although, most likely, such a hierarchy would be realized with realistic values for the couplings). Accordingly, we calculate all leading two-loop contributions, i.e., those that probe products of couplings that are not appearing in the one-loop contributions. (In the latter case, the two-loop diagrams would just constitute a small radiative correction to the leading one-loop result.)

Again, the full two-loop diagrams should only be used if no large logarithms appear in the result (this is the case, for instance, if the only virtual fermion in the loop is the top quark). The reason is – as in the case of one-loop contributions – that the large size of the QCD corrections requires the consistent summation of all large logarithms. If all logarithms are small (i.e. the loop function depends only on particle masses of the order of the electroweak scale), the full two-loop result is used as an initial condition for the EDM and chromo-EDM operators and the Weinberg operator, which then mix among each other when running to the hadronic scale. For instance, the loop function arising from diagrams with virtual bottom and charm quarks frequently exhibits a quadratic large logarithm of the form $\log^2(m_q/M_h)$, $q = b, c$. In this case, only the tree-level initial condition of the appropriate four-quark operator is needed. In fact, using the full two-loop result would lead to a large error (see Ref. [52] and the discussion in Sec. 4.2). In some cases, the two-loop result exhibits a *linear* large logarithm. In our context, this logarithm can be generated either via a threshold correction at a heavy-quark scale (this happens, for instance, for the bottom-quark contribution to the Weinberg operator), or via an one-loop initial condition and subsequent RG evolution to the hadronic scale (examples are fermionic Barr-Zee diagrams involving the exchange of virtual charged Higgs bosons, discussed in Sec. 4.1). In some cases, even QED effects have to be calculated to capture the leading effects. This is also discussed in Sec. 4.2.

In the following sections we define the effective five-, four-, and three-flavor Lagrangians, and discuss the renormalization group evolution between the weak scale and the low energy flavor thresholds, as well as the relevant threshold corrections.

3.1 Effective five- and four-flavor Lagrangians

The QCD corrections to the hadronic four-quark and dipole operators are large. Accordingly, we using RG-improved perturbation theory to sum all leading logarithms. The set of hadronic operators that contributes to the three-flavor Lagrangian via running and / or matching, and is closed under QCD RG, is

$$\begin{aligned}\mathcal{L}_{\text{eff,5f}} = & -\frac{1}{v^2}\sum_{q\neq q'}\left[\sum_{i=1,2} C_i^{qq'}Q_i^{qq'} + \frac{1}{2}\sum_{i=3,4} C_i^{qq'}Q_i^{qq'}\right] \\ & -\frac{1}{v^2}\sum_{q}\sum_{i=1}^{4}\left[C_i^q Q_i^q\right] - \frac{1}{v^2}C_w Q_w \\ & -\frac{1}{v^3}\sum_{q,\ell}\left[C_1^{\ell q}Q_1^{\ell q} + C_1^{q\ell}Q_1^{q\ell} + C_2^{\ell q}Q_2^{\ell q}\right] - \frac{1}{v^3}C_5^e Q_5^e\,.\end{aligned} \tag{10}$$

The summation runs over all leptons and quarks with masses below the weak scale ($\ell = e, \mu, \tau$; $q, q' = u, d, s, c, b$). The four-flavour effective Lagrangian can simply be obtained by excluding the bottom quark from the sum. The four-quark operators are defined as

$$Q_1^{qq'} = (\bar{q}q)\,(\bar{q}'\,i\gamma_5 q')\,, \qquad Q_2^{qq'} = (\bar{q}\,T^a q)\,(\bar{q}'\,i\gamma_5 T^a q')\,, \tag{11}$$

$$Q_3^{qq'} = \frac{1}{2}\epsilon^{\mu\nu\rho\sigma}(\bar{q}\sigma_{\mu\nu}q)\,(\bar{q}'\,\sigma_{\rho\sigma}q')\,, \qquad Q_4^{qq'} = \frac{1}{2}\epsilon^{\mu\nu\rho\sigma}(\bar{q}\sigma_{\mu\nu}T^a q)\,(\bar{q}'\sigma_{\rho\sigma}T^a q')\,, \tag{12}$$

$$Q_1^{q} = (\bar{q}q)\,(\bar{q}\,i\gamma_5 q)\,, \qquad Q_2^{q} = \frac{1}{2}\epsilon^{\mu\nu\rho\sigma}(\bar{q}\sigma_{\mu\nu}q)\,(\bar{q}\,\sigma_{\rho\sigma}q)\,, \tag{13}$$

and the semileptonic operators are

$$Q_1^{\ell q} = m_q(\bar{\ell}\ell)\,(\bar{q}\,i\gamma_5 q)\,,\qquad Q_1^{q\ell} = m_q(\bar{\ell}\,i\gamma_5\ell)\,(\bar{q}q)\,,\qquad Q_2^{\ell q} = \frac{m_q}{2}\epsilon^{\mu\nu\rho\sigma}(\bar{\ell}\sigma_{\mu\nu}\ell)\,(\bar{q}\,\sigma_{\rho\sigma}q)\,. \tag{14}$$

Here, $\epsilon^{\mu\nu\rho\sigma}$ is the completely antisymmetric Levi-Civita tensor, with sign convention $\epsilon_{0123}=1$, and we have defined $\sigma^{\mu\nu} = \frac{i}{2}[\gamma^\mu,\gamma^\nu]$. Note that we have included an explicit quark mass factor in the definition of the semileptonic operators, and a corresponding additional normalization factor of $1/v$ in the Lagrangian (10), to avoid ratios of quark and lepton masses in the anomalous dimensions of these operators, Eq. (28). Finally, we define the dimension-seven operator,

$$Q_5^e = \frac{\alpha_s}{12\pi}\bar{e}i\gamma_5 e\, G^a_{\mu\nu}G^{a,\mu\nu}\,. \tag{15}$$

It induces a CP-violating electron-nucleon coupling, and captures the effects of $Q_1^{b\ell}$ and $Q_1^{c\ell}$ at low energies, see Eq. (30).

The dipole operators are normalized in a way that gives a convenient form of the anomalous dimension. We use the following definitions,

$$Q_3^q = \frac{eQ_q}{2}\frac{m_q}{g_s^2}\,(\bar{q}\sigma^{\mu\nu}i\gamma_5 q)\,F_{\mu\nu}\,, \tag{16}$$

$$Q_4^q = -\frac{1}{2}\frac{m_q}{g_s}\,(\bar{q}\sigma^{\mu\nu}i\gamma_5 T^a q)\,G^a_{\mu\nu}\,, \tag{17}$$

$$Q_w = -\frac{1}{3g_s}f^{abc}\,G^a_{\mu\sigma}G^{b,\sigma}_{\nu}\widetilde{G}^{c,\mu\nu}\,. \tag{18}$$

Here, $F_{\mu\nu} = \partial_\mu A_\nu - \partial_\nu A_\mu$ and $G^a_{\mu\nu} = \partial_\mu G^a_\nu - \partial_\nu G^a_\mu + g_s f^{abc}G^b_\mu G^c_\nu$ are the field-strength tensors for QED and QCD, respectively. The dual gluon field strength tensor is defined as $\tilde{G}^{a,\mu\nu} = \frac{1}{2}\epsilon^{\mu\nu\alpha\beta}G^a_{\alpha\beta}$, with $\epsilon^{0123}=-1$. In our convention, the covariant derivative acting on quark fields is given by

$$D_\mu = \partial_u - ig_s T^a G^a_\mu + ieQ_q A_\mu\,. \tag{19}$$

Q_f is the charge of fermion f in units of the positron charge e. The basis of all CP-odd operators is closed under the RG flow of both QCD and QED as both interactions are CP conserving.

3.2 RG evolution

We define the anomalous dimensions via the RG equation for the Wilson coefficients,

$$\frac{dC_i}{d\log\mu} = \sum_j C_j\gamma_{ji}\,. \tag{20}$$

The explicit expressions for the QCD anomalous dimensions are collected in this section. (QED effects are discussed in Sec. 4.2.) We keep only the leading contributions in the strong coupling constant, expanding $\gamma = (\alpha_s/4\pi)\gamma^{(0)} + \ldots$.

The anomalous dimensions for the dipole and hadronic operators can be taken from Ref. [43] (the original references for the one-loop results are [39–42, 53]):

$$\gamma^{(0)}_{q\to q} = \begin{pmatrix} -10 & -\frac{1}{6} & 4 & 4 \\ 40 & \frac{34}{3} & -112 & -16 \\ 0 & 0 & -\frac{34}{3}+\frac{4}{3}N_f & 0 \\ 0 & 0 & \frac{32}{3} & -\frac{38}{3}+\frac{4}{3}N_f \end{pmatrix}, \tag{21}$$

$$\gamma^{(0)}_{qq'\to q} = \begin{pmatrix} 0 & 0 & 0 & 0 \\ 0 & 0 & 0 & 0 \\ 0 & 0 & 0 & 0 \\ 0 & 0 & 0 & 0 \\ 0 & 0 & -48\frac{Q_{q'}}{Q_q}\frac{m_{q'}}{m_q} & 0 \\ 0 & 0 & 0 & -8\frac{m_{q'}}{m_q} \end{pmatrix}, \tag{22}$$

$$\gamma^{(0)}_{qq'\to qq'} = \begin{pmatrix} -16 & 0 & 0 & 0 & 0 & -2 \\ 0 & 2 & 0 & 0 & -\frac{4}{9} & -\frac{5}{6} \\ 0 & 0 & -16 & 0 & 0 & -2 \\ 0 & 0 & 0 & 2 & -\frac{4}{9} & -\frac{5}{6} \\ 0 & -48 & 0 & -48 & \frac{16}{3} & 0 \\ -\frac{32}{3} & -20 & -\frac{32}{3} & -20 & 0 & -\frac{38}{3} \end{pmatrix}, \tag{23}$$

$$\gamma^{(0)}_{W\to q} = \begin{pmatrix} 0 & 0 & 0 & 6 \end{pmatrix}, \tag{24}$$

$$\gamma^{(0)}_{W\to W} = -8 + \frac{8}{3}N_f\,. \tag{25}$$

Here, N_f denotes the number of active quark flavors. In our matrix notation, we used the following ordering of the Wilson coefficients:

$$\begin{aligned} q &= \{C_1^q,\, C_2^q,\, C_3^q,\, C_4^q\}\,, \\ qq' &= \{C_1^{qq'},\, C_2^{qq'},\, C_1^{q'q},\, C_2^{q'q},\, C_3^{qq'},\, C_4^{qq'}\}\,. \end{aligned} \tag{26}$$

The semileptonic operators evolve like currents under QCD, see Ref. [44]. Using the results of Refs. [43, 54], we see that the scalar operators in Eq. (14) do not mix into the dipole operators Eqs. (16) and (17). The tensor operators in Eq. (14), on the other hand, do mix into the dipole operators. Their leading non-zero initial condition arise at one-loop for the tensor operators with up-type quarks (see Eq. (93), (94) below). This corresponds to the appearance of a large linear logarithm in some of the two-loop diagrams. Using the ordering

$$\ell q = \{C_1^{\ell q},\, C_1^{q\ell},\, C_2^{\ell q}\}\,, \tag{27}$$

we find the following anomalous dimensions [44])

$$\gamma^{(0)}_{\ell q\to \ell q} = \begin{pmatrix} 0 & 0 & 0 \\ 0 & 0 & 0 \\ 0 & 0 & \frac{32}{3} \end{pmatrix}, \qquad \gamma^{(0)}_{\ell q\to q} = \begin{pmatrix} 0 & 0 & 0 & 0 \\ 0 & 0 & 0 & 0 \\ 0 & 0 & -16\frac{Q_\ell}{Q_q}\frac{m_\ell}{v} & 0 \end{pmatrix}, \tag{28}$$

$$\gamma^{(0)}_{Q_e^5\to eq} = \begin{pmatrix} 0 & 0 & 0 \end{pmatrix}, \qquad \gamma^{(0)}_{Q_e^5\to Q_e^5} = 0\,. \tag{29}$$

The operator Q_e^5 mixes into the semileptonic operator $Q_1^{q\ell}$ at order α_s^2. The effect is numerically tiny, and we will neglect it. A detailed discussion of large logarithms arising from light fermion masses, including QED effects, is given in Sec. 4.2.

Finite contributions to the Wilson coefficients arise when crossing a heavy-flavor threshold. At the bottom-quark threshold, the coefficients of Q_5^e and the Weinberg operator receive a finite matching correction at leading order [39, 40, 54]

$$C_5^e|_{n_f=4}(\mu_b) = C_5^e|_{n_f=5}(\mu_b) - C_1^{be}|_{n_f=5}(\mu_b)\,, \tag{30}$$

$$C_w|_{n_f=4}(\mu_b) = C_w|_{n_f=5}(\mu_b) - \frac{\alpha_s^{(5)}}{8\pi} C_4^b|_{n_f=5}(\mu_b)\,. \tag{31}$$

An analogous contribution arises at the charm-quark threshold.

3.3 Effective three-flavor Lagrangian and dipole coefficients

After evolving all Wilson coefficients to the hadronic scale $\mu_{\rm had} = 2\,{\rm GeV}$, we slightly change the coefficients of the (chromo-)electric dipole operators to match the form used in evaluating the corresponding hadronic matrix elements, see Ref. [24]. We use the following CP-odd, flavor-conserving Lagrangian to parameterize the contributions to quark and gluon (chromo-)EDMs:

$$\begin{aligned}\mathcal{L}_{\rm dipole,3f} = &- \sum_{q=u,d,s} \frac{d_q}{2} (\bar q \sigma^{\mu\nu} i\gamma_5 q) F_{\mu\nu} - \sum_{q=u,d,s} \frac{g_s \tilde d_q}{2} (\bar q \sigma^{\mu\nu} i\gamma_5 T^a q) G^a_{\mu\nu} \\ &+ \frac{d_w}{3} f^{abc}\, G^a_{\mu\sigma} G^{b,\sigma}_{\nu} \widetilde G^{c,\mu\nu} + \dots\,.\end{aligned} \tag{32}$$

The ellipsis denotes the remaining, unchanged contributions in the three-flavor effective theory. (In particular, we do not change the definitions of the four-fermion operators.) The remaining operators have been defined in Eqs. (11)-(15); the summation here is over the light quarks only, $q = u, d, s$. The relation between the previously defined Wilson coefficients and the dipole moments for the hadronic EDMs is

$$d_q(\mu_{\rm had}) = \frac{1}{v^2} \frac{Q_q e}{4\pi\alpha_s} m_q C_3^q(\mu_{\rm had})\,, \tag{33}$$

$$\tilde d_q(\mu_{\rm had}) = -\frac{1}{v^2} \frac{1}{4\pi\alpha_s} m_q C_4^q(\mu_{\rm had})\,, \tag{34}$$

$$d_w(\mu_{\rm had}) = \frac{1}{v^2} \frac{1}{g_s} C_w^q(\mu_{\rm had})\,. \tag{35}$$

The strong coupling constant and all quark masses should be evaluated at $\mu_{\rm had} = 2\,{\rm GeV}$.

4 Weak-scale matching

In this section, we provide the explicit results for the matching conditions of the 2HDM described in Sec. 2 onto the five-flavor effective Hamiltonian (10). These matching conditions are the main results of this work. The Wilson coefficients are subsequently evolved to the hadronic scale using the RG equations, as explained in Sec. 3.2.

All Feynman diagrams have been calculated using the package `MaRTIn` [55], based on `FORM` [56] and implementing the algorithms developed in Refs. [57, 58]. The diagrams have been generated using `qgraf` [59], and typeset in latex using `jaxodraw` [60], based on `axodraw` [61]. We have calculated all diagrams in generalized R_ξ gauge for the photon and all weak gauge bosons [28], and explicitly verified the gauge-parameter independence of all our final results. The Feynman rules for the unphysical Goldstone bosons are taken from Ref. [62]. As a further check, all results have been obtained by at least two independent calculations.

The calculation of the two-loop diagrams with internal closed fermion loops (Fig. 2, left panel) involves the evaluation of fermion traces containing one or more powers of γ_5. For reasons of algebraic consistency, we employ the 't Hooft-Veltman scheme for γ_5, involving mixed

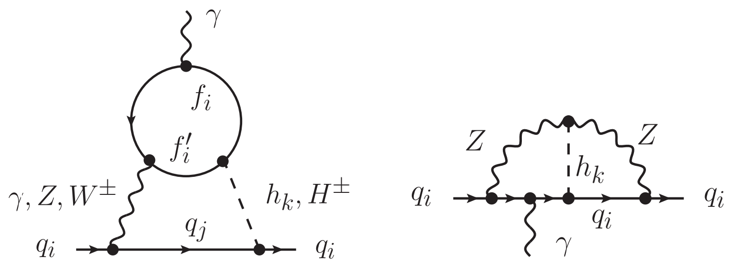

Figure 2: Representative two-loop diagrams contributing to the light-quark EDM.

commutation and anticommutation relations (see Ref. [63–65] for details). Our calculations are consistent with the available results in the literature, after the proper inclusion of finite counterterm contributions, as described in Ref. [28].

In all our results, we use the approximation of a unit CKM matrix. For all tree-level results (contained in Sec. 4.6 and Sec. 4.7) it is straightforward to include the effects of the full CKM matrix V by replacing $\rho_d \to \rho_d V^\dagger$ and $\rho_u \to V^\dagger \rho_u$ in the charged-Higgs contributions, cf. Eq. (7). In some of the loop-level contributions, this replacement (and the corresponding modifications of the charged weak currents) would imply additional quark mass dependence in the loop functions, so that not all those results can be easily generalized for a full CKM matrix. The terms that are neglected in our approximation are suppressed by small quark-mass to gauge- and Higgs-boson mass ratios and / or small off-diagonal CKM matrix elements. They are not expected to have a sizeable effects on the phenomenology.

We present the fermionic contributions to the quark electric dipole moments in Sec. 4.1. The contributions of light fermions that are enhanced by a large logarithm require a separate treatment, presented in Sec. 4.2. The bosonic contributions to the quark EDMs can be found in Sec. 4.3. We give only the results for the up, down, and strange EDMs (the charm and bottom EDMs would receive some additional contributions that we did not calculate). The quark chromo-EDMs and the contribution to the Weinberg operator are presented in Sec. 4.4 and Sec. 4.5, respectively. Finally, in Sec. 4.6 we present the contributions to the CP-violating four-quark operators, and in Sec. 4.7 the contributions to the semi-leptonic operators. All results presented in this section are new in the sense that, to the best of our knowledge, they have never been calculated in fully analytic form and for arbitrary phases in both the Higgs potential and the Yukawa couplings.

4.1 Fermionic contributions to the quark EDMs

We split the initial conditions at the weak scale into their one-loop and two-loop contributions; they should be summed to obtain the total result. Below the weak scale, additional contributions (corresponding to certain light-fermion loops) are generated by the RG evolution, see Sec. 4.2.

The only non-zero contributions at one-loop involve diagrams with internal top quarks. We find

$$C_3^{u_i,\text{one-loop}} = -\frac{\alpha_s}{4\pi}\frac{m_t}{m_{u_i}}\sum_k \frac{v^2}{M_{h_k}^2} g_1(x_{th_k}) \text{Im}\{\rho_{u,3i}^* \rho_{u,i3}^* q_{k2}^2\}\,, \tag{36}$$

$$C_3^{d_i,\text{one-loop}} = -\frac{\alpha_s}{4\pi}\frac{m_t}{m_{d_i}}\frac{v^2}{M_{H^\pm}^2}\big[4g_1(x_{tH^\pm}) + 3g_2(x_{tH^\pm})\big]\text{Im}\big\{\rho^*_{u,i3}\rho_{d,i3}\big\}\,. \tag{37}$$

Here and below, we define the squared mass ratios $x_{ab} \equiv M_a^2/M_b^2$. The one-loop functions are defined by

$$g_1(x) = \frac{x-3}{2(x-1)^2} + \frac{1}{(x-1)^3}\log x\,, \qquad g_2(x) = \frac{x+1}{(x-1)^2} - \frac{2x}{(x-1)^3}\log x\,. \tag{38}$$

It is convenient to split the two-loop contribution into several terms as follows. For the up-quark EDM, we have

$$\begin{aligned} C_3^{u,\text{two-loop}} &= C_3^{u,th} + C_3^{u,tH^\pm} + C_3^{u,cH^\pm} \\ &\quad + C_3^{u,hZ} + C_3^{u,\text{kin.}} + C_3^{u,H^\pm\gamma} + C_3^{u,H^\pm Z} + C_3^{u,H^\pm W}\,, \end{aligned} \tag{39}$$

and for the down- and strange-quarks EDMs, we have

$$\begin{aligned} C_3^{d_i,\text{two-loop}} &= C_3^{d_i,th} + C_3^{d_i,tH^\pm} + \sum_j C_3^{d_i,\ell_j H^\pm} \\ &\quad + C_3^{d_i,hZ} + C_3^{d_i,\text{kin.}} + C_3^{d_i,H^\pm\gamma} + C_3^{d_i,H^\pm Z} + C_3^{d_i,H^\pm W}\,. \end{aligned} \tag{40}$$

All the individual terms in these sums are separately gauge invariant. They correspond to Barr-Zee diagrams with internal top-quark loops and neutral Higgs bosons ($C_3^{u,th}$ and $C_3^{d_i,th}$), Barr-Zee diagrams with internal top-quark loops and charged Higgs bosons ($C_3^{u,tH^\pm}$ and $C_3^{d_i,tH^\pm}$), Barr-Zee diagrams with internal light fermion loops and charged Higgs bosons ($C_3^{u,cH^\pm}$ and $C_3^{d_i,\ell_j H^\pm}$), and non-Barr-Zee diagrams with internal Z and neutral Higgs bosons ($C_3^{u,hZ}$ and $C_3^{d_i,hZ}$). The remaining diagrams involve couplings from the Higgs kinetic terms ($C_3^{u,\text{kin.}}$ and $C_3^{d_i,\text{kin.}}$), as well as couplings from the Higgs potential ($C_3^{u,H^\pm V}$ and $C_3^{d_i,H^\pm V}$), with $V = \gamma, Z, W$. The explicit expressions for the various terms are given below.

The contributions of Barr-Zee diagrams with internal top-quark loops and neutral Higgs bosons (see Fig. 2, left panel) can be obtained by simple replacements from the results in Ref. [28]. We find for the down and strange EDMs ($d_1 = d$, $d_2 = s$)

$$\begin{aligned} C_3^{d_i,th} &= \frac{3\alpha\alpha_s Q_t}{4\pi^2}\frac{v^2}{m_{d_i}}\sum_{k=1}^{3}\frac{m_t}{M_{h_k}^2} \\ &\times\Bigg\{\Big[Q_t f_1(x_{th_k}) - \frac{v_u^Z v_d^Z}{4Q_d} f_3(x_{th_k}, x_{tZ})\Big]\text{Im}(\rho^*_{u,33}q_{k2})\Big(\frac{m_{d_i}}{v}q_{k1} + \text{Re}(\rho^*_{d,ii}q_{k2})\Big) \\ &\quad - \Big[Q_t f_2(x_{th_k}) - \frac{v_u^Z v_d^Z}{4Q_d} f_4(x_{th_k}, x_{tZ})\Big]\text{Im}(\rho^*_{d,ii}q_{k2})\Big(\frac{m_t}{v}q_{k1} + \text{Re}(\rho^*_{u,33}q_{k2})\Big)\Bigg\}\,, \end{aligned} \tag{41}$$

Here, $v_f^Z \equiv (T_3^f - 2Q_f s_w^2)/s_w c_w$ is the vectorial Z coupling to fermion f, and $T_3^f = \pm 1/2$ is the weak isospin of the fermion f. The result for the up-quark EDM, $C_3^{u,th}$, can be obtained by the replacements $m_{d_i} \to m_u$, $Q_d \to Q_u$, $v_d^Z \to v_u^Z$, and $\rho_{d,ii} \to \rho_{u,11}$, and changing the overall sign of the last line. The dimensionless two-loop functions appearing in this result are well-known [66]; they are given explicitly by

$$f_1(x) = \Phi\Big(\frac{1}{4x}\Big)\,, \qquad\qquad f_2(x) = (1-2x)f_1(x) + 2\big(2+\log(x)\big)\,, \tag{42}$$

$$f_3(x,y) = \frac{y}{x-y}\left[f_1(x) - f_1(y)\right], \qquad f_4(x,y) = \frac{y}{x-y}\left[f_2(x) - f_2(y)\right]. \tag{43}$$

The function $\Phi(x)$ is defined in Ref. [57].

All charged SM fermions other than the top quark will also contribute to the up- and down-quark EDMs. Inspection of the loop functions shows that they are, for small fermion masses, numerically dominated by powers of large logarithms of the form $\log(m_f^2/M_{h_k}^2)$; these logarithms need to be summed to all orders in the strong coupling constant. By contrast, naively using (41) in the limit of small fermion masses would lead to wrong results. This is explained in detail in Sec. 4.2.

Next, we discuss the contribution of diagrams with internal fermions and charged Higgs bosons (see Fig. 2, left panel). The result for the down-quark dipole is given, for internal top and bottom quarks:

$$\begin{aligned} C_3^{d_i,tH^\pm} = \frac{\alpha\alpha_s}{16\pi^2 s_w^2 Q_d}\frac{m_t v^2}{m_{d_i} M_{H^\pm}^2}\Big(&\mathrm{Im}\big(\rho_{u,33}\rho_{d,ii}^*\big) f_5(x_{tH^\pm}, x_{tW}) \\ &+ \frac{m_b}{m_t}\mathrm{Im}\big(\rho_{d,33}\rho_{d,ii}^*\big) f_6(x_{tH^\pm}, x_{tW})\Big). \end{aligned} \tag{44}$$

Here, the explicit expressions for the two-loop functions are

$$f_5(x,y) = \frac{y}{x-y}\left[\tilde{f}_5(x) - \tilde{f}_5(y)\right], \tag{45}$$

where

$$\tilde{f}_5(x) = 3x - \frac{1}{2}(13-6x)\log x + (2-x)(2-3x)\left[\mathrm{Li}_2(1-1/x) - \frac{\pi^2}{6}\right], \tag{46}$$

and

$$f_6(x,y) = \frac{y}{x-y}\left[\tilde{f}_6(x) - \tilde{f}_6(y)\right], \tag{47}$$

with

$$\tilde{f}_6(x) = -3x + \frac{1}{2}(1-6x)\log x + x(2-3x)\left[\mathrm{Li}_2(1-1/x) - \frac{\pi^2}{6}\right]. \tag{48}$$

The contribution to the down-quark EDM of diagrams with internal charged leptons is calculated by expanding to linear order in the lepton mass before performing the loop integrals. We find

$$C_3^{d_i,\ell_j H^\pm} = \frac{\alpha\alpha_s}{32\pi^2 s_w^2 Q_d}\frac{m_{\ell_j} v^2}{m_{d_i} M_{H\pm}^2}\mathrm{Im}\big(\rho_{\ell,jj}\rho_{d,ii}^*\big)\frac{1}{1-x_{WH^\pm}}\log x_{WH^\pm}. \tag{49}$$

The contribution of diagrams with a top or charm quark and charged Higgs bosons to the up-quark EDM is given by

$$C_3^{u,tH^\pm} = -\frac{\alpha\alpha_s}{16\pi^2 s_w^2 Q_u}\frac{m_t v^2}{m_u M_{H^\pm}^2}\mathrm{Im}\big(\rho_{u,33}\rho_{u,11}^*\big) f_6(x_{tH^\pm}, x_{tW}), \tag{50}$$

$$C_3^{u,cH^\pm} = -\frac{\alpha\alpha_s}{32\pi^2 s_w^2 Q_u}\frac{m_c v^2}{m_u M_{H^\pm}^2}\mathrm{Im}\big(\rho_{u,22}\rho_{u,11}^*\big)\frac{\log x_{WH^\pm}}{x_{WH^\pm}-1}. \tag{51}$$

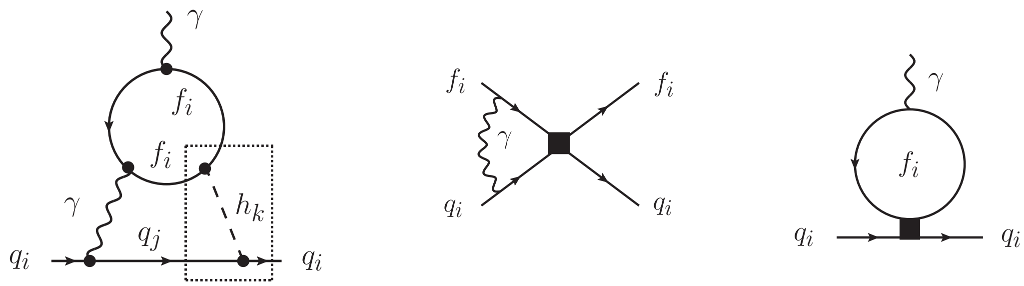

Figure 3: Integrating out the neutral Higgs bosons at tree level generates scalar four-fermion operators. They mix into tensor operators via one-loop photon exchange, and the tensor operators mix into the electric dipole operators. This generates the leading quadratic logarithms in Eq. (52). QCD RG evolution then sums the leading logarithms to all orders in α_s.

In the diagrams with charged Higgs bosons, the virtual charm-quark contributions to the down-quark EDM $C_3^{d_i}$, as well as the virtual lepton and bottom-quark contributions to the up-quark EDM C_3^u, lead to a large logarithm in the loop function that needs to be summed to all orders, similar to the case of diagrams with neutral Higgs bosons and light fermions, as discussed above. This is explained in detail in the following section.

4.2 Logarithmically enhanced light-fermion contributions to quark EDMs

The two-loop top-quark contribution (41) to the quark EDMs can, in principle, also be evaluated for the other quarks and charged leptons. However, in the limit of small fermion masses, the loop functions in Eqs. (42) and (43) contain large logarithms that needs to be properly summed to all orders in the strong coupling constant. One complication in this summation is that, for the photon contribution in Eq. (41), this logarithm arises from QED operator mixing. For the Z contribution, on the other hand, the logarithm arises from one-loop initial conditions to the tensor operators (12) and (14), and subsequent QCD mixing into the dipole operator. Similarly, a W box contribution to the tensor operators and subsequent QCD mixing into the dipole operator gives rise to a large logarithm in the Barr-Zee diagrams with charged Higgs bosons and virtual bottom quarks and leptons (for C_3^u), and with virtual charm quarks (for $C_3^{d_i}$). In the following, we discuss all these cases.

4.2.1 Photon contribution

The two-loop fermionic contributions to the quark EDMs, evaluated for internal lepton loops, would take the form

$$
\begin{aligned}
C_3^{d_i,\ell_j h} = & -\frac{\alpha\alpha_s}{4\pi^2}\frac{v^2}{m_{d_i}}\sum_{k=1}^{3}\frac{m_{\ell_j}}{M_{h_k}^2} \\
& \times\Bigg\{\left[f_1(x_{\ell h_k})+\frac{v_\ell^Z v_d^Z}{4Q_d}f_3(x_{\ell_j h_k},x_{\ell_j Z})\right]\mathrm{Im}(\rho^*_{\ell,jj}q_{k2})\left(\frac{m_{d_i}}{v}q_{k1}+\mathrm{Re}(\rho^*_{d,ii}q_{k2})\right) \\
& \quad +\left[f_2(x_{\ell h_k})+\frac{v_\ell^Z v_d^Z}{4Q_d}f_4(x_{\ell_j h_k},x_{\ell_j Z})\right]\mathrm{Im}(\rho^*_{d,ii}q_{k2})\left(\frac{m_{\ell_j}}{v}q_{k1}+\mathrm{Re}(\rho^*_{\ell,jj}q_{k2})\right)\Bigg\}\,.
\end{aligned}
\tag{52}
$$

(As before, the results for the up-quark EDM, $C_3^{u,\ell_j h}$, can be obtained by the replacements $m_{d_i} \to m_u$, $Q_d \to Q_u$, $v_d^Z \to v_u^Z$, and $\rho_{d,ii} \to \rho_{u,11}$, and changing the overall sign of the last line.) The leading asymptotic values of the loop functions for $x \ll 1$ and $y \ll 1$ are given by[2]

$$f_1(x) \simeq \log^2 x\,, \qquad\qquad f_2(x) \simeq \log^2 x\,, \tag{53}$$

$$f_3(x,y) \simeq \frac{y}{x-y}\big[\log x + \log y\big]\log\frac{x}{y}\,, \qquad f_4(x,y) \simeq \frac{y}{x-y}\big[\log x + \log y\big]\log\frac{x}{y}\,. \tag{54}$$

The large (linear and quadratic) logarithms should be summed to all orders in the strong coupling α_s. The photon and Z contributions are treated quite differently in the effective theory below the weak scale. The photon exchange generates quadratic logarithms $\log^2(m_{\ell_j}^2/M_{h_k}^2)$, via the mixing of the scalar operators $Q_1^{\ell_j q_i}$ and $Q_1^{q_i \ell_j}$ into the tensor operators $Q_2^{\ell_j q_i}$ through single-photon exchange, and subsequent mixing of $Q_2^{\ell_j q_i}$ into the electric dipole $Q_e^{q_i}$. This mixing chain is illustrated in Fig. 3. The linear large logarithms $\log(m_{\ell_j}^2/M_{h_k}^2)$ and $\log(m_{\ell_j}^2/M_Z^2)$ of the Z contribution, on the other hand, arise from a one-loop initial condition of the tensor operators $Q_2^{\ell_j q_i}$ at the weak scale, and subsequent mixing of $Q_2^{\ell_j q_i}$ into the electric dipole $Q_e^{q_i}$, see Fig. 4.

We start by discussing the photon case. After the RG evolution, the large logarithms will have the form $\log(\mu_{\rm had}^2/M_{h_k})$, with scale $\mu_{\rm had}$ of the order of 2 GeV where the hadronic matrix elements are evaluated. One sees immediately that a naive evaluation of the loop functions in the fixed-order result (52) can lead to a gross overestimation of the contribution: the result is "wrong" by a factor $\log^2[(2\,{\rm GeV})^2/m_\mu^2] \approx 35$ for the muon and $\log^2[(2\,{\rm GeV})^2/m_e^2] \approx 275$ for the electron.[3] Moreover, this neglects the large QCD effects that arise from the summation of the large logarithms.

The proper way of summing the large logarithms proceeds along the lines presented in Ref. [44]. The rationale of this calculation is the following. The limiting values of f_1 and f_2 in Eq. (53) can be reproduced as the leading term in a series that has the schematic form $\alpha\alpha_s \log^2(x_{\ell_j h_k})(1 + \alpha_s \log(x_{\ell_j h_k}) + \alpha_s^2 \log^2(x_{\ell_j h_k}) + \ldots)$. Here, the first term reflects the quadratic logarithm in Eq. (53), while all other terms correspond to the leading logarithms of the diagrams obtained by dressing the Barr-Zee diagrams, Fig. 2, with an arbitrary number of virtual gluons. We use the formalism of Ref. [67] to resum the large logarithms $\alpha_s \log(x_{\ell_j h_k})$ to all orders.

The required entries of the QED anomalous dimensions are given by (cf. Ref. [44])

$$\gamma_{C_1^{\ell q} \to C_2^{\ell q}} = \gamma_{C_1^{q\ell} \to C_2^{\ell q}} = \frac{\alpha}{2\pi} Q_q + \ldots\,. \tag{55}$$

Other entries of the semileptonic anomalous dimension matrix are either zero or numerically irrelevant. The ellipsis denotes QCD and higher-order contributions. The exact leading-logarithmic result for charged-lepton contributions to the electric dipole Wilson coefficient

[2] The loop functions for small fermion masses are numerically dominated by the leading logarithms. The next-leading terms in the expansion are $\pi^2/3$ for $f_1(x)$, a relative correction of 0.5%, 1.6%, 4.5% for an internal electron, muon, and tau, respectively; and $2\log(x)$ for $f_2(x)$, corresponding to a relative correction of the order of ten percent. (Here we assume that $M_{h_k} \geq 125\,$GeV for all three neutral Higgs bosons.) The subleading corrections to $f_3(x,y)$ and $f_4(x,y)$ are tiny. In all cases, it is a good approximation to keep only the (RG-improved) leading-logarithmic contribution.

[3] The electron case is phenomenologically not very relevant, as the electron-Higgs couplings receive much stronger constraints from bounds on the electron EDM, discussed in Ref. [28].

is simple enough to be written out in the following compact form:

$$
\begin{aligned}
C_3^{q_i,\ell_j h}(\mu_{\rm had}) = \Big[&\frac{12}{115}\eta_3^{-11/27}\eta_4^{-9/25}\eta_5^{-7/23} - \frac{144}{4025}\eta_3^{-11/27}\eta_4^{-9/25}\eta_5^{16/23} \\
&- \frac{16}{525}\eta_3^{-11/27}\eta_4^{16/25}\eta_5^{16/23} - \frac{8}{21}\eta_3^{16/27}\eta_4^{16/25}\eta_5^{16/23} \\
&+ \frac{48}{2975}\eta_3^{-11/27}\eta_4^{-9/25}\eta_5 + \frac{32}{4725}\eta_3^{-11/27}\eta_4^{16/25}\eta_5 \\
&+ \frac{16}{189}\eta_3^{16/27}\eta_4^{16/25}\eta_5 + \frac{80}{8721}\eta_3^{-11/27}\eta_4\eta_5 \\
&+ \frac{16}{297}\eta_3^{16/27}\eta_4\eta_5 + \frac{36}{209}\eta_3\eta_4\eta_5\Big]\frac{\alpha}{\alpha_s^{(5)}(m_t)}\frac{m_{\ell_j}}{v}\left[C_1^{\ell_j q_i}(m_t) + C_1^{q_i\ell_j}(m_t)\right] ,
\end{aligned} \tag{56}
$$

where $\eta_5 = \alpha_s^{(5)}(m_t)/\alpha_s^{(5)}(m_b)$, $\eta_4 = \alpha_s^{(4)}(m_b)/\alpha_s^{(4)}(m_c)$, and $\eta_3 = \alpha_s^{(3)}(m_c)/\alpha_s^{(3)}(\mu_{\rm had})$; the superscript denotes the number of active quark flavors. The initial conditions for the Wilson coefficients are given in Eqs. (91) and (92), below. It is straightforward to check that this solution exactly reproduces the quadratic large logarithm in Eq. (52).

The bottom and charm contributions to the light-quark EDMs are obtained in a completely analoguous way. The only required, non-zero entries of the QED anomalous dimension matrix are

$$
\gamma_{C_1^{qq'}\to C_3^{qq'}} = \gamma_{C_1^{q'q}\to C_3^{qq'}} = -\frac{\alpha}{2\pi}Q_qQ_{q'} + \dots . \tag{57}
$$

Again, all other entries are not needed, and we indicate QCD and higher-order terms by the ellipsis. The initial conditions are required for the coefficients C_1^{ub}, C_1^{bu}, $C_1^{d_id_3}$, $C_1^{d_3d_i}$ for virtual bottom quarks, and C_1^{uc}, C_1^{cu}, $C_1^{d_ic}$, $C_1^{cd_i}$ for virtual charm quarks. They are given explicitly in Eqs. (81), (82), and (87).[4]

The structure of the anomalous dimensions for virtual bottom and charm quarks is more complicated than in the semi-leptonic case, and it is not instructive to present the analytic result explicitly. Needless to say, the corresponding solution of the RG equation is included in the python code.

4.2.2 Z- and W-boson contributions

The leading-logarithmic contribution of virtual Z bosons to the quark EDMs with virtual bottom, charm, and lepton loops is obtained via the one-loop initial conditions for the four-quark and semileptonic tensor operators, given in Eqs. (84), (85), (89), (93), and (94), respectively, and subsequent QCD RG evolution (mixing of the tensor operators into the electric dipole operators). The "mixing chain" is explained in Fig. 4.

Similarly, one obtains the leading-logarithmic contribution of virtual W bosons to the quark EDMs with virtual bottom, charm, and lepton loops via the one-loop initial conditions for the four-quark and semileptonic tensor operators, given in Eqs. (84), (85), (93), and (94), respectively. The exceptions are the bottom and lepton contributions to the down- and strange-quark EDMs, and the charm contribution to the up-quark EDM. For these particular flavor combinations, the tensor operators do not mix into the dipole operators, and no large logarithm appears

[4]Here and in the following, we do not need to consider the contributions of virtual up, down, and strange quarks, as their couplings receive much stronger contraints from contributions to the up-, down-, and strange-quark EDMs arising from *heavy* virtual particles (e.g. via top-loop or bosonic Barr-Zee diagrams).

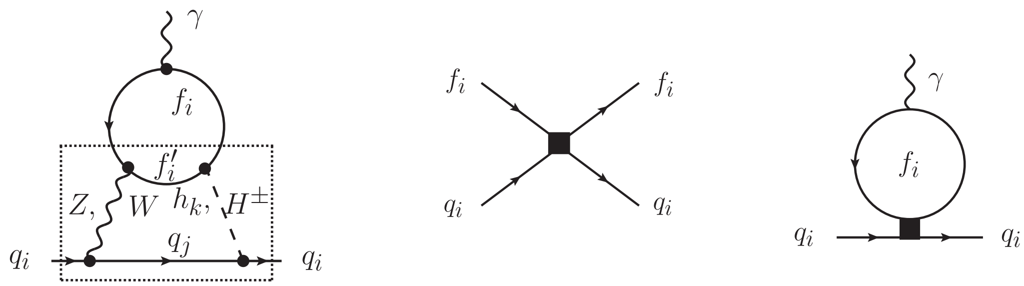

Figure 4: Integrating out the Higgs, W, and Z bosons at one-loop generates tensor four-fermion operators. They mix into the electric dipole operators. This generates the leading linear logarithms in Eq. (52). QCD RG evolution then sums the leading logarithms to all orders in α_s.

in the two-loop functions. The two-loop results can then directly be used as initial conditions for the RG evolution; the corresponding expressions have been given in Eqs. (44), (51), and (49).

4.2.3 One-loop contributions

The function g_1 appearing in the one-loop top-quark contributions (36) and (37) to the quark EDMs is also proportional to a large logarithm for the case of internal bottom and charm quarks, corresponding to the left and right panels in Fig. 1 with charm and bottom quarks instead of top quark. (Also the corresponding diagrams with external down and strange quarks need to be taken into account.) This logarithm is reproduced and summed to all orders by the RG evolution, starting with the tree-level initial conditions (84), (85), and (89) for the tensor four-quark operators, and subsequent mixing into the electric dipole operators.

4.3 Bosonic contributions to the quark EDMs

In this section we present the contributions from diagrams involving vertices arising from the kinetic terms of the Higgs bosons and the Higgs potential. Among the diagrams with vertices from the Higgs kinetic terms only, there are two classes that are separately gauge invariant. The first class consists of the diagrams with internal Z and neutral Higgs bosons that are not of the Barr-Zee type (see Fig. 2, right panel):

$$\begin{aligned} C_3^{d_i,hZ} = & \frac{e\alpha\alpha_s\left(v_d^Z\right)^2}{96\pi^2 s_w c_w}\frac{v^2}{m_{d_i}M_Z}\sum_{k=2}^{3} q_{k1}\mathrm{Im}\left(\rho_{d,ii}^* q_{k2}\right)\left[f_{7+}(x_{Zh_k}) - f_{7+}(x_{Zh_1})\right] \\ & + \frac{e\alpha\alpha_s\left(a_d^Z\right)^2}{96\pi^2 s_w c_w}\frac{v^2}{m_{d_i}M_Z}\sum_{k=2}^{3} q_{k1}\mathrm{Im}\left(\rho_{d,ii}^* q_{k2}\right)\left[f_{7-}(x_{Zh_k}) - f_{7-}(x_{Zh_1})\right], \end{aligned} \tag{58}$$

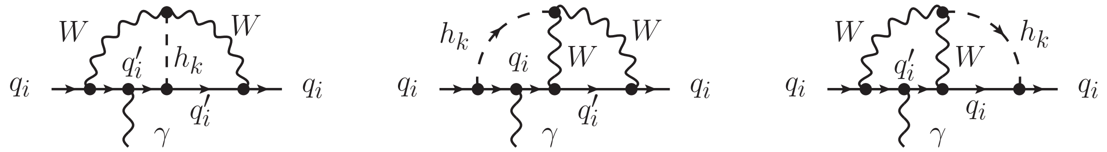

Figure 5: Representative non-Barr-Zee two-loop diagrams with W exchange contributing to the light-quark EDM. The external photon can be attached to any internal charged line. The four diagrams represented by the left panel have no correspondence in the electron EDM case; they turn out to be zero.

where $a_f^Z \equiv -T_3^f/(s_w c_w)$ is the axial Z coupling to fermion f. The loop functions are

$$\begin{aligned} f_{7\pm}(x) = \; & \frac{16x^4 + 4x^3 - (2 \pm 24)x^2 \pm (18x - 3)}{4x^3}\Phi\left(\frac{1}{4x}\right) + \frac{8x^2 - 2x \mp 3}{2x} \\ & - \frac{4x^5 + 3x^4 - (1 \pm 3)x^2 \pm (12x - 3)}{x^3}\,\mathrm{Li}_2(1-x) - \frac{8x^5 + 6x^4 \mp (12x - 3)}{12x^3}\pi^2 \\ & - \log^2(x)\frac{8x^5 + 6x^4 - (2 \pm 6)x^2 \pm (12x - 3)}{4x^3} + \log(x)\frac{4x^2 + x \pm 3}{x}\,. \end{aligned} \tag{59}$$

The dilogarithm is defined as

$$\mathrm{Li}_2(x) = -\int_0^x du\, \log(1-u)/u\,. \tag{60}$$

The result for the up-quark EDM, $C_3^{u,hZ}$, can be obtained by the replacements $m_{d_i} \to m_u$, $v_d^Z \to v_u^Z$, $a_d^Z \to a_u^Z$, and $\rho_{d,ii} \to \rho_{u,11}$, and changing the overall sign.

All remaining diagrams with vertices from the Higgs kinetic terms give

$$\begin{aligned} C_3^{d_i,\mathrm{kin.}} = \; & \frac{e\alpha\alpha_s v_d^Z}{64\pi^2 Q_d}\frac{v^2}{m_{d_i}M_Z}\sum_{k=2}^{3} q_{k1}\mathrm{Im}\big(\rho_{d,ii}^* q_{k2}\big)\left[f_{12a}(x_{Zh_k}, c_w^2) - f_{12a}(x_{Zh_1}, c_w^2)\right] \\ & - \frac{e\alpha\alpha_s}{32\pi^2 s_w}\frac{v^2}{m_{d_i}M_W}\sum_{k=2}^{3} q_{k1}\mathrm{Im}\big(\rho_{d,ii}^* q_{k2}\big)\left[f_{8c}(x_{Wh_k}) - f_{8c}(x_{Wh_1})\right] \\ & + \frac{e\alpha\alpha_s}{144\pi^2 s_w^3 Q_d}\frac{v^2}{m_{d_i}M_W}\sum_{k=2}^{3} q_{k1}\mathrm{Im}\big(\rho_{d,ii}^* q_{k2}\big)\left[f_{12b}(x_{Wh_k}) - f_{12b}(x_{Wh_1})\right] \\ & + \frac{e\alpha\alpha_s}{64\pi^2 Q_d s_w^3}\frac{v^2}{m_{d_i}M_W}\sum_{k=2}^{3} q_{k1}\mathrm{Im}\big(\rho_{d,ii}^* q_{k2}\big)\left[f_{8e}(x_{Wh_k}, x_{WH^+}) - f_{8e}(x_{Wh_1}, x_{WH^+})\right]. \end{aligned} \tag{61}$$

The four lines in Eq. (61) correspond to Barr-Zee-type diagrams (one Higgs and one gauge boson coupling to the external quark) with internal Z-boson exchange (first line), Barr-Zee-type diagrams with internal photon exchange (second line), diagrams with internal W-boson exchange that are not of the Barr-Zee type (one Higgs and two gauge bosons coupling to the external quark, see diagrams in Fig. 5 – third line), Barr-Zee-type diagrams with internal W-boson exchange (fourth line). Note that this splitting is not entirely physical, as it depends on the choice of gauge parameter. Only in the sum of all contributions and after using the orthogonality conditions of the Higgs mixing angles the gauge parameters drop out, as we verified explicitly (see also App. B). The gauge-independent parts of the loop functions are given by (the somewhat idiosyncratic naming of the loop functions is to avoid inconsistency with the naming of loop functions in Ref. [28])

$$\begin{aligned} f_{12a}(x,y) &= \frac{12xy^2-16xy+3x}{(1-x)(1-y)}\,\Phi\left(\frac{1}{4y}\right) - \frac{12x^2y^2-16xy+3}{(1-x)(1-y)}\Phi\left(\frac{1}{4xy}\right) \\ &\quad + \log(x)\frac{12xy^2-2xy+2y-1}{(1-x)(1-y)y}\,, \end{aligned} \tag{62}$$

$$f_{8c}(x) = \big(12x^2-16x+3\big)\Phi\left(\frac{1}{4x}\right) - 2\big[\log(x)+2\big]\big(6x+1\big) \tag{63}$$

$$\begin{aligned} f_{12b}(x) &= \frac{4x^2+3x}{12}\pi^2 + \log^2(x)\frac{4x^3+3x^2-1}{x} - \log(x)\big(2x+5\big) \\ &\quad + \frac{8x^4+6x^3-2x-9}{4x^2}\mathrm{Li}_2(1-x) \\ &\quad + \frac{38x^3-49x^2-16x+9}{8x^2}\Phi\left(\frac{1}{4x}\right) - \frac{8x-11}{4}\,, \end{aligned} \tag{64}$$

$$\begin{aligned} f_{8e}(x,y) &= \log^2(x)\frac{x^3y(3-y)+3x^2y^2-x(3y^2+4y+1)+y^2+y}{2x^3} \\ &\quad + \log(x)\log(y)\frac{x^3y(y^2-4y+3)-3x^2y^2(y-1)+xy^2(3y+1)-y^3}{2x^3(y-1)} \\ &\quad + \log(x)\frac{y-xy-x}{x^2} + \log(y)\frac{x^2(1+7y-2y^2)+xy(4y+1)-2y^2}{2x^2(y-1)} \\ &\quad + \left[\frac{x^4y(3-y^3+5y^2-7y)+x^3y^3(4y-8)}{2x^4(y-1)}\right. \\ &\qquad \left. - \frac{x^2y^2(6y^2-y+1)-xy^3(4y+2)+y^4}{2x^4(y-1)}\right]\Phi\left(y,\frac{y}{x}\right) \\ &\quad + \frac{x^3y(3-y)+3x^2y^2-xy(3y+4)+y(y+1)}{x^3}\mathrm{Li}_2(1-x) \\ &\quad + \frac{4x^3+6x^2-6x+1}{2x^3(y-1)}\,y\,\Phi\left(\frac{1}{4x}\right) + \frac{xy(2-x)+x-y}{x^2}\,. \end{aligned} \tag{65}$$

The function $\Phi(x,y)$ is defined in Ref. [57]. For the up-quark EDM we find

$$\begin{aligned} C_3^{u,\mathrm{kin.}} &= -\frac{e\alpha\alpha_s v_u^Z}{64\pi^2 Q_u}\frac{v^2}{m_u M_Z}\sum_{k=2}^{3} q_{k1}\mathrm{Im}\big(\rho_{u,ii}^* q_{k2}\big)\big[f_{12a}(x_{Zh_k},c_w^2)-f_{12a}(x_{Zh_1},c_w^2)\big] \\ &\quad + \frac{e\alpha\alpha_s}{32\pi^2 s_w}\frac{v^2}{m_u M_W}\sum_{k=2}^{3} q_{k1}\mathrm{Im}\big(\rho_{u,ii}^* q_{k2}\big)\big[f_{8c}(x_{Wh_k})-f_{8c}(x_{Wh_1})\big] \\ &\quad + \frac{e\alpha\alpha_s}{144\pi^2 s_w^3 Q_u}\frac{v^2}{m_u M_W}\sum_{k=2}^{3} q_{k1}\mathrm{Im}\big(\rho_{u,ii}^* q_{k2}\big)\big[f_{12c}(x_{Wh_k})-f_{12c}(x_{Wh_1})\big] \\ &\quad + \frac{e\alpha\alpha_s}{64\pi^2 Q_u s_w^3}\frac{v^2}{m_u M_W}\sum_{k=2}^{3} q_{k1}\mathrm{Im}\big(\rho_{u,ii}^* q_{k2}\big)\big[f_{8e}(x_{Wh_k},x_{WH^+})-f_{8e}(x_{Wh_1},x_{WH^+})\big]\,, \end{aligned} \tag{66}$$

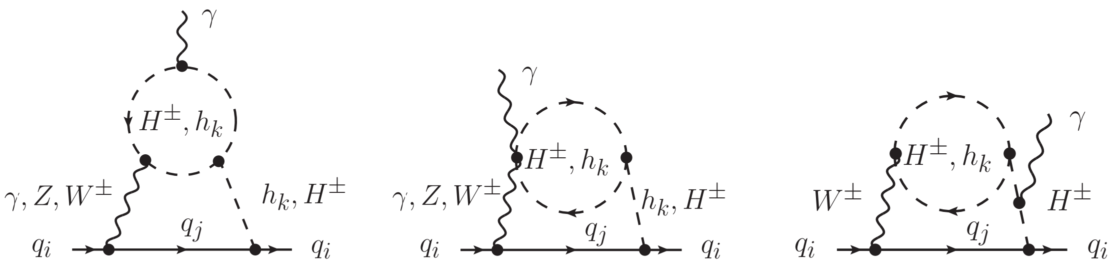

Figure 6: Representative two-loop diagrams contributing to the light-quark EDM with vertices arising from the Higgs potential.

where

$$
\begin{aligned}
f_{12c}(x) = {} & \frac{4x^2+3x}{6}\pi^2 + \log^2(x)\frac{4x^3+3x^2-1}{2x} - \log(x)\frac{8x+11}{2} \\
& + \frac{16x^4+12x^3-4x-9}{4x^2}\mathrm{Li}_2(1-x) \\
& + \frac{22x^3-53x^2-14x+9}{8x^2}\Phi\left(\frac{1}{4x}\right) - \frac{16x-13}{4}\,.
\end{aligned} \tag{67}
$$

Last, we discuss the contributions of diagrams with vertices derived from the Higgs potential. Such contribution necessarily enter at the two-loop level (see Fig. 6). The contribution of diagrams with internal photons and charged Higgs bosons is

$$
C_3^{d_i,H^\pm\gamma} = -\frac{\alpha\alpha_s}{8\pi^2}\sum_{k=1}^{3}\frac{v^3}{m_{d_i}M_{h_k}^2}\mathrm{Im}\big(\rho^*_{d,ii}q_{k2}\big)\Big[q_{k1}Z_3 + \mathrm{Re}(q_{k2}Z_7)\Big]f_9(x_{H^\pm h_k})\,, \tag{68}
$$

with the loop function

$$
f_9(x) = x\,\Phi\left(\frac{1}{4x}\right) - \log(x) - 2\,. \tag{69}
$$

The contribution of diagrams with internal Z bosons and charged Higgs bosons is

$$
C_3^{d_i,H^\pm Z} = \frac{\alpha\alpha_s}{32\pi^2}\frac{c_w^2-s_w^2}{s_w c_w Q_d}v_d^Z\sum_{k=1}^{3}\frac{v^3}{m_{d_i}M_{h_k}^2}\mathrm{Im}\big(\rho^*_{d,ii}q_{k2}\big)\Big[q_{k1}Z_3 + \mathrm{Re}(q_{k2}Z_7)\Big]f_{10}(x_{H^\pm h_k}, x_{Zh_k})\,, \tag{70}
$$

with

$$
f_{10}(x,y) = \frac{1}{1-y}\left[\log(y) - x\,\Phi\left(\frac{1}{4x}\right) + \frac{x}{y}\Phi\left(\frac{y}{4x}\right)\right]. \tag{71}
$$

The contribution of diagrams with internal W bosons and charged Higgs bosons is

$$
C_3^{d_i,H^\pm W} = \frac{\alpha\alpha_s}{64\pi^2 s_w^2 Q_d}\sum_{k=1}^{3}\frac{v^3}{m_{d_i}M_{h_k}^2}\mathrm{Im}\big(\rho^*_{d,ii}q_{k2}\big)\Big[q_{k1}Z_3 + \mathrm{Re}(q_{k2}Z_7)\Big]f_{11}(x_{H^\pm h_k}, x_{Wh_k})\,, \tag{72}
$$

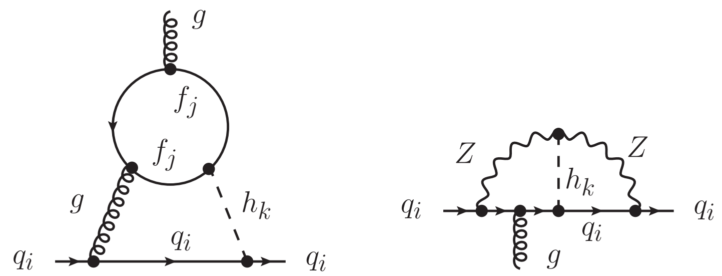

Figure 7: Representative two-loop diagrams contributing to the light-quark chromo-EDM.

with

$$
\begin{aligned}
f_{11}(x,y) = {} & \log(x)\log(y)\frac{yx - x^2 + 2x - 1}{y^2(y-x)} + \log(y)\frac{2x - y - 2}{y(y-x)} \\
& + \log^2(x)\frac{2x-1}{x^2(x-y)} + \log(x)\frac{yx + 2y - 2x^2}{xy(y-x)} + \frac{2(x-1)}{yx} \\
& + \frac{2yx^2 - y^2x - yx - y - x^3 + 3x^2 - 3x + 1}{y^2x(y-x)}\Phi\left(\frac{y}{x}, \frac{1}{x}\right) \\
& + \frac{2(y - 2yx + x^3 - 2x^2 + x)}{y^2x^2}\mathrm{Li}_2(1-x) + \frac{2x^2 - 4x + 1}{x^2(x-y)}\Phi\left(\frac{1}{4x}\right) .
\end{aligned}
\tag{73}
$$

The three contributions are separately gauge invariant. The contribution of all diagrams with internal Z bosons and vertices from the Higgs potential that do not contain charged Higgs bosons are zero. The results for the up-quark EDM, $C_3^{u,H^\pm\gamma}$, $C_3^{u,H^\pm Z}$, and $C_3^{u,H^\pm W}$, can be obtained by the replacements $m_{d_i} \to m_u$, $Q_{d_i} \to Q_u$, $v_d^Z \to v_u^Z$, and $\rho_{d,ii} \to \rho_{u,11}$, and changing the overall sign for $C_3^{u,H^\pm\gamma}$ and $C_3^{u,H^\pm Z}$, *but not for* $C_3^{u,H^\pm W}$.

4.4 Contributions to the quark chromo-EDMs

Here, we present the initial conditions for the chromo-EDMs of the up, down, strange, charm and bottom quarks. The charm and bottom chromo-EDMs are needed because they contribute to the coefficient of the Weinberg operator via finite threshold corrections, see Eq. (31). It is useful to split $C_4^{q_i}$ into a fermionic and a bosonic contribution, $C_4^{q_i} = C_4^{q_i,\text{fermionic}} + C_4^{q_i,\text{bosonic}}$. We find, for $d_1 = d$, $d_2 = s$, $d_3 = b$,

$$
\begin{aligned}
C_4^{d_i,\text{fermionic}} = {} & \frac{\alpha_s}{2\pi}\frac{m_t}{m_{d_i}}\frac{v^2}{M_{H^\pm}^2} g_1(x_{tH^\pm})\mathrm{Im}\big(\rho_{u,i3}^*\rho_{d,i3}\big) \\
& - \frac{\alpha_s^2}{8\pi^2}\frac{m_t}{m_{d_i}}\sum_{k=1}^{3}\frac{v^2}{M_{h_k}^2}\bigg\{ \quad f_1(x_{th_k})\mathrm{Im}(\rho_{u,33}^* q_{k2})\Big(\frac{m_{d_i}}{v}q_{k1} + \mathrm{Re}(\rho_{d,ii}^* q_{k2})\Big) \\
& \qquad - f_2(x_{th_k})\mathrm{Im}(\rho_{d,ii}^* q_{k2})\Big(\frac{m_t}{v}q_{k1} + \mathrm{Re}(\rho_{u,33}^* q_{k2})\Big)\bigg\} .
\end{aligned}
\tag{74}
$$

For the up-quark ($u_1 = u$, $u_2 = c$) chromo-electric dipoles, we find

$$\begin{aligned}
C_4^{u_i,\text{fermionic}} &= -\frac{\alpha_s}{4\pi}\frac{m_t}{m_{u_i}}\sum_k \frac{v^2}{M_{h_k}^2} g_1(x_{th_k})\text{Im}\{\rho^*_{u,3i}\rho^*_{u,i3}q_{k2}^2\} \\
&\quad - \frac{\alpha_s^2}{8\pi^2}\frac{m_t}{m_{u_i}}\sum_{k=1}^{3}\frac{v^2}{M_{h_k}^2}\Bigg\{ \quad f_1(x_{th_k})\text{Im}(\rho^*_{u,33}q_{k2})\Big(\frac{m_{u_i}}{v}q_{k1} + \text{Re}(\rho^*_{u,ii}q_{k2})\Big) \\
&\qquad\qquad + f_2(x_{th_k})\text{Im}(\rho^*_{u,ii}q_{k2})\Big(\frac{m_t}{v}q_{k1} + \text{Re}(\rho^*_{u,33}q_{k2})\Big)\Bigg\}.
\end{aligned} \tag{75}$$

The first lines in Eqs. (74) and (75) correspond to the one-loop contribution (see middle panel in Fig. 1); the second and third lines represent the contributions of gluonic Barr-Zee diagrams with internal top-quark loops and neutral Higgs bosons (see Fig. 7, left panel). They can be obtained by simple replacements of couplings and charges (and dropping the Z contribution) from the results for the electric dipole, Eq. (41). The dimensionless two-loop functions appearing in this result have been given above, Eq. (42).

It should be obvious that these contributions to the chromo-EDMs of the light quarks are numerically much larger than the corresponding contributions (with photons instead of gluons) to the electric dipole moments. In fact, the contributions to the electric dipole moments that are induced, via QCD RG running, from chromo-electric dipole moments typically dominate by large factors over the direct contributions, discussed in the previous sections. Note, however, that diagrams with virtual leptons or with vertices from the Higgs potential do not contribute to the chromo-EDMs and are only tested via the electric dipole moments.

The result for the non-Barr-Zee Z and W contributions is

$$C_4^{d_i,\text{bosonic}} = -C_3^{d_i,hZ} + \frac{\alpha\alpha_s e}{96\pi^2 s_w^3}\frac{v^2}{M_W m_{d_i}}\sum_{k=1}^{3} q_{k1}\text{Im}\big(\rho^*_{d,ii}q_{k2}\big)f_{13}(x_{Wh_k}), \tag{76}$$

where the loop function is

$$\begin{aligned}
f_{13}(x) &= 1 - 4x - (4x+1)\log(x) - \frac{8x^2+2x-1}{2x}\Phi\Big(\frac{1}{4x}\Big) \\
&\quad + \frac{4x^3+3x^2-1}{2x}\big[\log^2(x) + 2\text{Li}_2(1-x)\big] + \frac{4x^2+3x}{6}\pi^2.
\end{aligned} \tag{77}$$

The result for the up- and charm-quark EDMs, $C_4^{u_i,\text{bosonic}}$, can be obtained by the replacements $C_3^{d_i,hZ} \to C_3^{u_i,hZ}$, and changing $m_{d_i} \to m_u$, $\rho_{d,ii} \to \rho_{u,11}$, as well as the overall sign, in the second term.

Light-quark contributions

Contributions of virtual quarks other than the top are taken into account via the mixing of scalar and tensor four-quark operators into the chromo-electric dipole, in analogy to the case of electric dipoles, described in detail in Sec. 4.2. In particular, the large quadratic logarithm that appears in the two-loop contribution in Eqs. (74) and (75) when replacing the top quark with bottom or charm quarks can be reproduced and summed to all orders in QCD, using the initial conditions for the scalar four-quark operators, Eqs. (81), (82), and (87), and subsequent

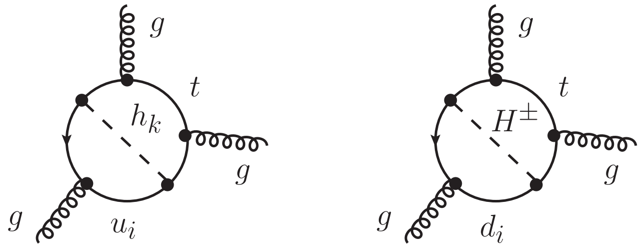

Figure 8: Representative two-loop diagrams contributing to the gluon chromo-EDM ("Weinberg operator").

mixing into the tensor and chromo-electric dipole operators. This chain can again be illustrated with Fig. 3, where one should now replace all photons by gluons.[5]

Similarly, the large logarithm in the one-loop contribution in Eqs. (74) and (75), evaluated for virtual bottom and charm quarks, is reproduced and summed to all orders in QCD, using the initial conditions for the tensor four-quark operators, starting with the tree-level initial conditions (84), (85), and (89), and subsequent mixing into the chromo-electric dipole operators.

4.5 Contributions to the Weinberg operator

The contribution of the Weinberg operator to hadronic EDMs is generally small [24]. Its significance arises from the fact that it receives contributions that are proportional to the (modified) top-quark Yukawa coupling only. These contributions arise from two-loop diagrams involving virtual top quarks, see Fig. 8. The corresponding initial conditions are

$$\begin{aligned} C_w^h = &-\frac{\alpha_s^2}{32\pi^2}\sum_k \frac{v^2}{M_{h_k}^2}\Big[\mathrm{Im}\big((\rho_{u,33}^*)^2 q_{k2}^2\big) + \frac{2m_t}{v} q_{k1}\mathrm{Im}\big(\rho_{u,33}^* q_{k2}\big)\Big] f_{14}(x_{th_k}) \\ &- \frac{\alpha_s^2}{32\pi^2}\sum_k \frac{v^2}{M_{h_k}^2}\sum_{i=1,2}\Big[\mathrm{Im}\big(\rho_{u,i3}^*\rho_{u,3i}^* q_{k2}^2\big) + \frac{m_t}{v} q_{k1}\mathrm{Im}\big(\rho_{u,i3}^* q_{k2}\big)\Big] f_{15}(x_{th_k}) \\ &- \frac{\alpha_s^2}{16\pi^2}\frac{v^2}{M_{H^\pm}^2}\sum_{i=1}^{3}\mathrm{Im}\big(\rho_{d,i3}^*\rho_{u,i3}\big) f_{15}(x_{tH^\pm}) \,, \end{aligned} \tag{78}$$

where (cf. the results in Ref. [66])

$$f_{14}(x) = \frac{6x^2-5x-1}{(4x-1)^3}\log x - \frac{2x-3}{2(4x-1)^2} - \frac{6x^3-6x^2+3x}{(4x-1)^3}\Phi(1/4x)\,, \tag{79}$$

$$f_{15}(x) = \frac{x}{(x-1)^4}\log x + \frac{x^2-5x-2}{6(x-1)^3}\,. \tag{80}$$

Note that the Weinberg operator receives additional logarithmically enhanced contributions from finite threshold corrections at the bottom- and charm-quark scales. Again, the most significant are those arising from the bottom-quark contribution to the bottom-quark chromo-EDM, and the charm-quark contribution to the charm-quark chromo-EDM, see Sec. 3.2. In analogy to the top-quark contributions, they are respectively proportional to modifications of

[5]Higher-order resummation of these logarithms has been performed in Ref. [43].

the bottom- and charm-quark Yukawas only. They are additional finite contributions, at the weak scale as well as at the bottom and charm thresholds, arising from two-loop diagrams with virtual light quarks, analoguos to those shown in Fig. 8 (and corresponding diagrams where the Higgs propoagators are replaced by insertions of effective four-quark operators). All these contributions are proportional to combinations of couplings that are already probed by contributions to the quark (chromo-)EDMs that have much larger hadronic matrix elements. Hence, we neglect these contributions to the Weinberg operator.

4.6 Contributions to four-quark operators

We calculate the matching conditions at the weak scale for all four-quark operators in our basis. While their direct contribution to hadronic CP violation is negligible (their hadronic matrix elements are tiny, see Ref. [24]), they mix into the (chromo-)electric dipole operators and thus account for the CP violation induced by virtual light quarks, as explained in Sec. 4.2.

The following Wilson coefficients receive their leading contributions at tree-level:

$$C_1^{u_i d_j} = -\sum_k \frac{v^2}{M_{h_k}^2}\Big(\frac{m_{u_i}}{v}q_{k1} + \mathrm{Re}\big(\rho_{u,ii}^* q_{k2}\big)\Big)\mathrm{Im}\big(\rho_{d,jj}^* q_{k2}\big) - \frac{1}{6}\frac{v^2}{M_{H^\pm}^2}\mathrm{Im}\big(\rho_{d,ji}^*\rho_{u,ji}\big)\,, \tag{81}$$

$$C_1^{d_i u_j} = \sum_k \frac{v^2}{M_{h_k}^2}\Big(\frac{m_{d_i}}{v}q_{k1} + \mathrm{Re}\big(\rho_{d,ii}^* q_{k2}\big)\Big)\mathrm{Im}\big(\rho_{u,jj}^* q_{k2}\big) - \frac{1}{6}\frac{v^2}{M_{H^\pm}^2}\mathrm{Im}\big(\rho_{d,ij}^*\rho_{u,ij}\big)\,, \tag{82}$$

$$C_2^{u_i d_j} = C_2^{d_j u_i} = 2C_4^{u_i d_j} = -\frac{v^2}{M_{H^\pm}^2}\mathrm{Im}\big(\rho_{d,ji}^*\rho_{u,ji}\big)\,. \tag{83}$$

The operator $Q_3^{u_i d_j}$, on the other hand, receives contributions both at tree-level and at one-loop. The relevance of the one-loop contributions has been explained in Sec. 4.2. Note in particular that the tree-level and one-loop contributions depend on different Higgs coupling combinations. For $j = 1, 2$, we find

$$\begin{aligned} C_3^{u_i d_j} = &-\frac{v^2}{12 M_{H^\pm}^2}\mathrm{Im}\big(\rho_{d,ji}^*\rho_{u,ji}\big) \\ &+ \frac{\alpha}{16\pi s_w^2}\frac{v^2}{M_{H^\pm}^2}\mathrm{Im}\big(\rho_{u,ii}\rho_{d,jj}^*\big)\frac{\log x_{WH^\pm}}{x_{WH^\pm}-1} \\ &+ \frac{\alpha v_u^Z v_d^Z}{16\pi}\sum_k \frac{v^2}{M_{h_k}^2}\frac{\log x_{Zh_k}}{1-x_{Zh_k}} \\ &\times \Big[\mathrm{Im}\big(\rho_{u,ii}\rho_{d,jj}^*\big)|q_{k2}|^2 - \frac{m_{d_j}}{v}q_{k1}\mathrm{Im}\big(\rho_{u,ii}^* q_{k2}\big) + \frac{m_{u_i}}{v}q_{k1}\mathrm{Im}\big(\rho_{d,jj}^* q_{k2}\big)\Big]\,, \end{aligned} \tag{84}$$

while for $d_j = b$, we find

$$\begin{aligned}
C_3^{u_i b} &= -\frac{v^2}{12 M_{H^\pm}^2} \mathrm{Im}\big(\rho_{d,3i}^* \rho_{u,3i}\big) \\
&\quad + \frac{\alpha}{16\pi s_w^2} \frac{v^2}{M_{H^\pm}^2} \mathrm{Im}\big(\rho_{u,ii} \rho_{d,33}^*\big) f_{16}(x_{WH^\pm}, x_{tH^\pm}) \\
&\quad + \frac{\alpha v_u^Z v_d^Z}{16\pi} \sum_k \frac{v^2}{M_{h_k}^2} \frac{\log x_{Zh_k}}{1 - x_{Zh_k}} \\
&\qquad \times \left[\mathrm{Im}\big(\rho_{u,ii} \rho_{d,33}^*\big) |q_{k2}|^2 - \frac{m_b}{v} q_{k1} \mathrm{Im}\big(\rho_{u,ii}^* q_{k2}\big) + \frac{m_{u_i}}{v} q_{k1} \mathrm{Im}\big(\rho_{d,33}^* q_{k2}\big) \right],
\end{aligned} \tag{85}$$

with the loop function

$$f_{16}(x, y) = \frac{x \log x}{x^2 - xy - x + y} + \frac{y \log y}{y^2 - xy + x - y}\,. \tag{86}$$

Furthermore, for $i \neq j$ we find

$$C_1^{q_i q_j} = \pm \sum_k \frac{v^2}{M_{h_k}^2} \left\{ \Big(\frac{m_{q_i}}{v} q_{k1} + \mathrm{Re}(\rho_{q,ii}^* q_{k2}) \Big) \mathrm{Im}(\rho_{q,jj}^* q_{k2}) + \frac{1}{12} \mathrm{Im}\big(\rho_{q,ij}^* \rho_{q,ji}^* q_{k2}^2\big) \right\}, \tag{87}$$

$$C_2^{q_i q_j} = C_2^{q_j q_i} = 2 C_4^{q_i q_j} = \mp \frac{1}{2} \sum_k \frac{v^2}{M_{h_k}^2} \mathrm{Im}\big(\rho_{q,ij}^* \rho_{q,ji}^* q_{k2}^2\big)\,, \tag{88}$$

$$\begin{aligned}
C_3^{q_i q_j} &= \mp \frac{1}{24} \sum_k \frac{v^2}{M_{h_k}^2} \mathrm{Im}\big(\rho_{q,ij}^* \rho_{q,ji}^* q_{k2}^2\big) \\
&\quad \pm \frac{\alpha \big(v_q^Z\big)^2}{16\pi} \sum_k \frac{v^2}{M_{h_k}^2} \frac{\log x_{Zh_k}}{x_{Zh_k} - 1} \\
&\qquad \times \left[\mathrm{Im}\big(\rho_{q,ii}^* \rho_{q,jj}^*\big) |q_{k2}|^2 + \frac{m_{q_j}}{v} q_{k1} \mathrm{Im}\big(\rho_{q,ii}^* q_{k2}\big) + \frac{m_{q_i}}{v} q_{k1} \mathrm{Im}\big(\rho_{q,jj}^* q_{k2}\big) \right].
\end{aligned} \tag{89}$$

Here, the upper signs are for $q_i = u_i$ and the lower signs for $q_i = d_i$. And finally, for the operators with four equal quarks, we have

$$C_1^{q_i} = \pm \sum_k \frac{v^2}{M_{h_k}^2} \Big(\frac{m_{q_i}}{v} q_{k1} + \mathrm{Re}(\rho_{q,ii}^* q_{k2}) \Big) \mathrm{Im}\big\{\rho_{q,ii}^* q_{k2}\big\}\,, \tag{90}$$

with, again, the upper sign for $q_i = u_i$ and the lower sign for $q_i = d_i$. The coefficient $C_2^{q_i}$ receives a contribution from box diagrams with virtual Z and neutral Higgs bosons, but they are not phenomenologically relevant.

To obtain some of the results in this section, we used the Fierz identities collected in App. A. The naive application of these four-dimensional relations is permitted, since we are only calculating leading-logarithmic effects.

4.7 Contributions to semi-leptonic operators

Semi-leptonic four-fermion operators play a two-fold role in our analysis. They directly induce CP-violating electron-quark interactions, which translate into CP-violating electron-nucleon interactions that can be probed by measuring the EDMs of paramagnetic atoms and molecules [24]. In addition, they mix into the quark electric dipole operators and thus account for the CP violation induced by virtual charged leptons, as explained in Sec. 4.2.

The matching calculation at the weak scale gives the following results:

$$C_1^{\ell_i q_j} = \pm \sum_k \Big(\frac{v^2}{M_{h_k}^2} \frac{m_{\ell_i}}{m_{q_j}} q_{k1} + \frac{v^3}{M_{h_k}^2 m_{q_j}} \mathrm{Re}(\rho_{\ell,ii}^* q_{k2}) \Big) \mathrm{Im}(\rho_{q,jj}^* q_{k2}) \,, \tag{91}$$

$$C_1^{q_i \ell_j} = - \sum_k \Big(\frac{v^2}{M_{h_k}^2} q_{k1} + \frac{v^3}{M_{h_k}^2 m_{q_i}} \mathrm{Re}(\rho_{q,ii}^* q_{k2}) \Big) \mathrm{Im}(\rho_{\ell,jj}^* q_{k2}) \,. \tag{92}$$

Here, the upper sign applies for $q_i = u_i$ and the lower sign for $q_i = d_i$. At one-loop, also the tensor operators get generated:

$$\begin{aligned} C_2^{\ell_i u_j} &= \frac{\alpha}{16\pi s_w^2} \frac{v^3}{M_{H^\pm}^2 m_{u_j}} \mathrm{Im}\big(\rho_{\ell,ii} \rho_{u,jj}^*\big) \frac{\log x_{WH^\pm}}{1 - x_{WH^\pm}} \\ &\quad + \frac{\alpha v_\ell^Z v_u^Z}{16\pi} \sum_k \frac{v^3}{M_{h_k}^2 m_{u_j}} \frac{\log x_{Zh_k}}{1 - x_{Zh_k}} \\ &\quad \times \bigg[\mathrm{Im}\big(\rho_{\ell,ii}^* \rho_{u,jj}\big) |q_{k2}|^2 - \frac{m_{\ell_i}}{v} q_{k1} \mathrm{Im}\big(\rho_{u,jj}^* q_{k2}\big) + \frac{m_{u_j}}{v} q_{k1} \mathrm{Im}\big(\rho_{\ell,ii}^* q_{k2}\big) \bigg] \,, \end{aligned} \tag{93}$$

$$\begin{aligned} C_2^{\ell_i d_j} &= \frac{\alpha v_\ell^Z v_d^Z}{16\pi} \sum_k \frac{v^3}{M_{h_k}^2 m_{d_j}} \frac{\log x_{Zh_k}}{1 - x_{Zh_k}} \\ &\quad \times \bigg[\mathrm{Im}\big(\rho_{\ell,ii}^* \rho_{d,jj}^* q_{k2}^2\big) + \frac{m_{\ell_i}}{v} q_{k1} \mathrm{Im}\big(\rho_{d,jj}^* q_{k2}\big) + \frac{m_{d_j}}{v} q_{k1} \mathrm{Im}\big(\rho_{\ell,ii}^* q_{k2}\big) \bigg] \,. \end{aligned} \tag{94}$$

The initial condition for the CP-violating electron-gluon operator (15) arises at one-loop and is given by

$$C_5^e = - \sum_k \left(\frac{v^2}{M_{h_k}^2} q_{k1} + \frac{v^3}{M_{h_k}^2 m_t} \mathrm{Re}(\rho_{u,33}^* q_{k2}) \right) \mathrm{Im}(\rho_{\ell,11}^* q_{k2}) \,. \tag{95}$$

5 Conclusion

We presented the leading contributions to the light-quark ($q = u, d, s$) EDMs and chromo-EDMs, as well as to the Weinberg operator and CP-odd semileptonic four-fermion operators, in the unconstrained 2HDM. We kept terms that are at most quadratic in the Yukawa interactions. To the best of our knowledge, these results have been presented here in full generality for the first time. We paid particular attention to consistently summing all large logarithms using QCD and QED RG evolution using an low-energy effective theory. The corresponding RG evolution of the Wilson coefficients is valid not only for the 2HDM, but generally for any model that does not introduce new light degrees of freedom beyond the SM.

We verified our results through several consistency checks. We confirmed that all infrared and ultraviolat divergences cancel in our results. Moreover, we performed the calculation in generalized R_ξ gauge for all gauge bosons, and verified explicitly that all our results are gauge parameter independent.

Our results can be used to calculate the contributions in the 2HDM to EDMs of various nuclear, atomic, and molecular systems, see Ref. [24].

Python code

To make it easier to use our results in numerical applications, we provide an implementation of our results into `python` code. It can be downloaded via the public git repository

https://gitlab.com/jbrod/general-2hdm-pheno

and provides (in addition to the results of Ref. [28]) the numerical values for all Wilson coefficients at the hadronic scale $\mu = 2\,\text{GeV}$, and the values of the quark and gluon (chromo-)EDMs as defined in Sec. 3.3, for user-specified model input parameters. Information on the usage of the code can be found in the repository.

Acknowledgments

J.B. acknowledges support by DoE grant DE-SC0011784. The research of W.A. is supported by the U.S. Department of Energy grant number DE-SC0010107. The work of P.U. is supported in part by Thailand NSRF via PMU-B under grant number B39G680009.

A Fierz relations

We used the following Fierz identities to project onto our basis:

$$\begin{aligned}(\bar{q}q')\,(\bar{q}'\,i\gamma_5 q) + (\bar{q}'q)\,(\bar{q}\,i\gamma_5 q') &= -\frac{1}{6}\Big(Q_1^{qq'} + Q_1^{q'q}\Big) - \Big(Q_2^{qq'} + Q_2^{q'q}\Big) \\ &\quad - \frac{1}{12}Q_3^{qq'} - \frac{1}{2}Q_4^{qq'} - \frac{1}{12}Q_3^{qq'} - \frac{1}{2}Q_4^{qq'}\,,\end{aligned}\tag{96}$$

$$\begin{aligned}(\bar{q}\,T^a q')\,(\bar{q}'\,i\gamma_5 T^a q) + (\bar{q}'\,T^a q)\,(\bar{q}\,i\gamma_5 T^a q') &= -\frac{2}{9}\Big(Q_1^{qq'} + Q_1^{q'q}\Big) + \frac{1}{6}\Big(Q_2^{qq'} + Q_2^{q'q}\Big) \\ &\quad - \frac{1}{9}Q_3^{qq'} + \frac{1}{12}Q_4^{qq'}\,,\end{aligned}\tag{97}$$

$$\begin{aligned}\frac{1}{2}\epsilon^{\mu\nu\rho\sigma}(\bar{q}\sigma_{\mu\nu}q')\,(\bar{q}'\sigma_{\rho\sigma}q) &= -\Big(Q_1^{qq'} + Q_1^{q'q}\Big) - 6\Big(Q_2^{qq'} + Q_2^{q'q}\Big) \\ &\quad + \frac{1}{6}Q_3^{qq'} + Q_4^{qq'}\,,\end{aligned}\tag{98}$$

$$\begin{aligned}\frac{1}{2}\epsilon^{\mu\nu\rho\sigma}(\bar{q}\sigma_{\mu\nu}T^a q')\,(\bar{q}'\sigma_{\rho\sigma}T^a q) &= -\frac{4}{3}\Big(Q_1^{qq'} + Q_1^{q'q}\Big) + \Big(Q_2^{qq'} + Q_2^{q'q}\Big) \\ &\quad + \frac{2}{9}Q_3^{qq'} - \frac{1}{6}Q_4^{qq'}\,.\end{aligned}\tag{99}$$

The structures $(\bar{q}q')\,(\bar{q}'\,i\gamma_5 q) - (\bar{q}'q)\,(\bar{q}\,i\gamma_5 q')$ and $(\bar{q}\,T^a q')\,(\bar{q}'\,i\gamma_5 T^a q) - (\bar{q}'\,T^a q)\,(\bar{q}\,i\gamma_5 T^a q')$ are CP even and do not mix into the CP-odd operators. Hence, they do not contribute to EDMs. For the case of four equal quarks, we have two more relations:

$$(\bar{q}T^a q)\,(\bar{q}\,i\gamma_5 T^a q) \quad = \quad -\frac{5}{12}Q_1^q - \frac{1}{16}Q_2^q\,,\tag{100}$$

$$\frac{1}{2}\epsilon^{\mu\nu\rho\sigma}(\bar{q}\sigma_{\mu\nu}T^a q)\,(\bar{q}\sigma_{\rho\sigma}T^a q) \quad = \quad -3Q_1^q + \frac{1}{12}Q_2^q\,.\tag{101}$$

B Gauge-parameter dependent parts of the bosonic loop functions

As the bosonic contributions to the quark EDMs have been calculated here for the first time (part of the contributions can be extracted from the results in Ref. [33]), we show the gauge-parameter dependent parts of the loop functions (62)-(65) explicitly. It is straightforward to verify that all these contributions cancel in the sum, after applying unitarity relations.

$$\begin{aligned}
f_{12a,\xi}(x,y) =\ & \log(\xi)\log(x)\frac{xy\xi(2-\xi)-xy+\xi+3}{y-1} + \log(\xi)\log(y)\frac{xy\xi(2-\xi)-xy}{y-1} \\
& + \frac{x^2y^2(\xi^3-3\xi^2+3\xi-1)-xy(2\xi^2+2\xi-4)+\xi-3}{y-1}\Phi(xy,xy\xi) \\
& + \frac{2xy\xi^2-\xi}{y-1}\Phi(1/4xy\xi) + \frac{2xy(\xi^2-2\xi+1)}{y-1}\mathrm{Li}_2(1-\xi)\,,
\end{aligned} \tag{102}$$

$$\begin{aligned}
f_{8c,\xi}(x) =\ & \big(2x\xi^2-\xi\big)\Phi\left(\frac{1}{4x\xi}\right) + 2x\big(\xi^2-2\xi+1\big)\mathrm{Li}_2(1-\xi) \\
& + \big(x^2\xi^3-3x^2\xi^2+3x^2\xi-x^2-2x\xi^2-2x\xi+4x+\xi-3\big)\Phi\Big(x,x\xi\Big) \\
& - 2\log\xi + \xi\log^2\xi - \big(x\xi^2-2x\xi+x-\xi-3\big)\log\xi\log x\,,
\end{aligned} \tag{103}$$

$$\begin{aligned}
f_{12b,\xi}(x) =\ & 9\log x\log\xi\frac{x^3\xi^2-2x^3\xi+x^3+x^2\xi^2-2x^2\xi-3x^2-2x\xi+1}{8x^2} \\
& + 9\log^2(x)\frac{x\xi^2-x\xi-2\xi}{8x} + \frac{9\xi}{8}\log^2\xi - (1+\log\xi)\frac{9\xi}{4} \\
& + 9\frac{-x\xi^2+2x\xi-x}{4}\mathrm{Li}_2(1-\xi) + 9\frac{x^2\xi^2-x^2\xi-2x\xi+1}{4x^2}\mathrm{Li}_2(1-x\xi) \\
& + 9\frac{-2x\xi^2+\xi}{8}\Phi\left(\frac{1}{4x\xi}\right) \\
& + 9\Bigg[\frac{-3x^2\xi^2+3x^2+3x\xi+x-1}{8x^2} \\
& \quad + \frac{-x^2\xi^3+3x^2\xi^2-3x^2\xi+x^2+x\xi^3+3x\xi-4x}{8}\Bigg]\Phi\Big(x,x\xi\Big)\,,
\end{aligned} \tag{104}$$

$$\begin{aligned}
f_{8e,\xi}(x,y) =\ & \log(x)^2\frac{-x\xi^2+x\xi+2\xi}{2x} + \log(\xi)\log(x)\frac{-x^2\xi^2+x^2\xi+2x\xi-1}{2x^2} \\
& - \xi\log(\xi) - \xi + \mathrm{Li}_2(1-x\xi)\frac{-x^2\xi^2+x^2\xi+2x\xi-1}{x^2} \\
& + \Phi(x,x\xi)\frac{-x^3\xi^3+2x^3\xi^2-x^3\xi+3x^2\xi^2-x^2\xi-3x\xi-x+1}{2x^2}\,,
\end{aligned} \tag{105}$$

$$f_{12c,\xi}(x) = f_{12b,\xi}(x)\,. \tag{106}$$

References

[1] V. A. Kuzmin, V. A. Rubakov and M. E. Shaposhnikov, *On the Anomalous Electroweak Baryon Number Nonconservation in the Early Universe*, Phys. Lett. B **155** (1985) 36.

[2] N. G. Deshpande and E. Ma, *Pattern of Symmetry Breaking with Two Higgs Doublets*, Phys. Rev. D **18** (1978) 2574.

[3] S. J. Huber, M. Pospelov and A. Ritz, *Electric dipole moment constraints on minimal electroweak baryogenesis*, *Phys. Rev. D* **75** (2007) 036006, [hep-ph/0610003].

[4] J. de Vries, M. Postma, J. van de Vis and G. White, *Electroweak Baryogenesis and the Standard Model Effective Field Theory*, *JHEP* **01** (2018) 089, [1710.04061].

[5] J. De Vries, M. Postma and J. van de Vis, *The role of leptons in electroweak baryogenesis*, *JHEP* **04** (2019) 024, [1811.11104].

[6] K. Fuyuto, W.-S. Hou and E. Senaha, *Cancellation mechanism for the electron electric dipole moment connected with the baryon asymmetry of the Universe*, *Phys. Rev. D* **101** (2020) 011901, [1910.12404].

[7] S.-F. Ge, G. Li, P. Pasquini and M. J. Ramsey-Musolf, *CP-violating Higgs Di-tau Decays: Baryogenesis and Higgs Factories*, *Phys. Rev. D* **103** (2021) 095027, [2012.13922].

[8] E. Fuchs, M. Losada, Y. Nir and Y. Viernik, *CP violation from τ, t and b dimension-6 Yukawa couplings - interplay of baryogenesis, EDM and Higgs physics*, *JHEP* **05** (2020) 056, [2003.00099].

[9] H. Bahl, E. Fuchs, S. Heinemeyer, J. Katzy, M. Menen, K. Peters et al., *Constraining the $\mathcal{CP}$ structure of Higgs-fermion couplings with a global LHC fit, the electron EDM and baryogenesis*, *Eur. Phys. J. C* **82** (2022) 604, [2202.11753].

[10] P. Athron, M. J. Ramsey-Musolf, C. Sierra and Y. Wu, *Electroweak baryogenesis from charged current anomalies in B meson decays*, 2502.00445.

[11] W. Bernreuther, *CP violation and baryogenesis*, *Lect. Notes Phys.* **591** (2002) 237–293, [hep-ph/0205279].

[12] D. E. Morrissey and M. J. Ramsey-Musolf, *Electroweak baryogenesis*, *New J. Phys.* **14** (2012) 125003, [1206.2942].

[13] G. C. Dorsch, S. J. Huber and J. M. No, *A strong electroweak phase transition in the 2HDM after LHC8*, *JHEP* **10** (2013) 029, [1305.6610].

[14] P. Basler, M. Mühlleitner and J. Wittbrodt, *The CP-Violating 2HDM in Light of a Strong First Order Electroweak Phase Transition and Implications for Higgs Pair Production*, *JHEP* **03** (2018) 061, [1711.04097].

[15] J. O. Andersen, T. Gorda, A. Helset, L. Niemi, T. V. I. Tenkanen, A. Tranberg et al., *Nonperturbative Analysis of the Electroweak Phase Transition in the Two Higgs Doublet Model*, *Phys. Rev. Lett.* **121** (2018) 191802, [1711.09849].

[16] J. Bernon, L. Bian and Y. Jiang, *A new insight into the phase transition in the early Universe with two Higgs doublets*, *JHEP* **05** (2018) 151, [1712.08430].

[17] P. Basler and M. Mühlleitner, *BSMPT (Beyond the Standard Model Phase Transitions): A tool for the electroweak phase transition in extended Higgs sectors*, *Comput. Phys. Commun.* **237** (2019) 62–85, [1803.02846].

[18] M. Aoki, T. Komatsu and H. Shibuya, *Possibility of a multi-step electroweak phase transition in the two-Higgs doublet models*, *PTEP* **2022** (2022) 063B05, [2106.03439].

[19] P. Basler, L. Biermann, M. Mühlleitner and J. Müller, *Electroweak baryogenesis in the CP-violating two-Higgs doublet model*, *Eur. Phys. J. C* **83** (2023) 57, [2108.03580].

[20] H. Song, W. Su and M. Zhang, *Electroweak phase transition in 2HDM under Higgs, Z-pole, and W precision measurements*, *JHEP* **10** (2022) 048, [2204.05085].

[21] C. E. M. Wagner, *Electroweak Baryogenesis and Higgs Physics*, *LHEP* **2023** (2023) 466, [2311.06949].

[22] Anisha, F. Arco, S. Di Noi, C. Englert and M. Mühlleitner, *Z and Higgs Factory Implications of Two Higgs Doublets with First-Order Phase Transitions*, *JHEP* **10** (2025) 179, [2506.18555].

[23] K. Radchenko Serdula, *Unlocking the Higgs Potential: from Colliders to the Cosmos*, Ph.D. thesis, U. Hamburg (main), U. Hamburg (main), 2025.

[24] J. Engel, M. J. Ramsey-Musolf and U. van Kolck, *Electric Dipole Moments of Nucleons, Nuclei, and Atoms: The Standard Model and Beyond*, *Prog. Part. Nucl. Phys.* **71** (2013) 21–74, [1303.2371].

[25] S. Inoue, M. J. Ramsey-Musolf and Y. Zhang, *CP-violating phenomenology of flavor conserving two Higgs doublet models*, *Phys. Rev. D* **89** (2014) 115023, [1403.4257].

[26] T. Chupp, P. Fierlinger, M. Ramsey-Musolf and J. Singh, *Electric dipole moments of atoms, molecules, nuclei, and particles*, *Rev. Mod. Phys.* **91** (2019) 015001, [1710.02504].

[27] M. Pospelov and A. Ritz, *Electric Dipole Moments and New Physics*, 2509.23531.

[28] W. Altmannshofer, B. Assi, J. Brod, N. Hamer, J. Julio, P. Uttayarat et al., *Electron EDM and $\Gamma(\mu \to e\gamma)$ in the 2HDM*, *JHEP* **06** (2025) 156, [2410.17313].

[29] J. M. Dávila, A. Karan, E. Passemar, A. Pich and L. Vale Silva, *The Electric Dipole Moment of the electron in the decoupling limit of the aligned two-Higgs doublet model*, *JHEP* **10** (2025) 053, [2504.16700].

[30] S. Davidson and H. E. Haber, *Basis-independent methods for the two-Higgs-doublet model*, *Phys. Rev.* **D72** (2005) 035004, [hep-ph/0504050].

[31] H. E. Haber and D. O'Neil, *Basis-independent methods for the two-Higgs-doublet model. II. The Significance of tanβ*, *Phys. Rev. D* **74** (2006) 015018, [hep-ph/0602242].

[32] R. Boto, T. V. Fernandes, H. E. Haber, J. C. Romão and J. a. P. Silva, *Basis-independent treatment of the complex 2HDM*, *Phys. Rev. D* **101** (2020) 055023, [2001.01430].

[33] W. Altmannshofer, S. Gori, N. Hamer and H. H. Patel, *Electron EDM in the complex two-Higgs doublet model*, *Phys. Rev. D* **102** (2020) 115042, [2009.01258].

[34] A. Denner, G. Weiglein and S. Dittmaier, *Application of the background field method to the electroweak standard model*, *Nucl. Phys. B* **440** (1995) 95–128, [hep-ph/9410338].

[35] Flavour Lattice Averaging Group (FLAG) collaboration, Y. Aoki et al., *FLAG Review 2024*, 2411.04268.

[36] W. Buchmuller and D. Wyler, *Effective Lagrangian Analysis of New Interactions and Flavor Conservation*, *Nucl. Phys. B* **268** (1986) 621–653.

[37] B. Grzadkowski, M. Iskrzynski, M. Misiak and J. Rosiek, *Dimension-Six Terms in the Standard Model Lagrangian*, *JHEP* **10** (2010) 085, [1008.4884].

[38] F. Feruglio, *The Chiral approach to the electroweak interactions*, *Int. J. Mod. Phys. A* **8** (1993) 4937–4972, [hep-ph/9301281].

[39] E. Braaten, C.-S. Li and T.-C. Yuan, *The Evolution of Weinberg's Gluonic CP Violation Operator*, *Phys. Rev. Lett.* **64** (1990) 1709.

[40] E. Braaten, C. S. Li and T. C. Yuan, *The Gluon Color - Electric Dipole Moment and Its Anomalous Dimension*, *Phys. Rev. D* **42** (1990) 276–278.

[41] G. Degrassi, E. Franco, S. Marchetti and L. Silvestrini, *QCD corrections to the electric dipole moment of the neutron in the MSSM*, *JHEP* **11** (2005) 044, [hep-ph/0510137].

[42] J. Hisano, K. Tsumura and M. J. S. Yang, *QCD Corrections to Neutron Electric Dipole Moment from Dimension-six Four-Quark Operators*, *Phys. Lett. B* **713** (2012) 473–480, [1205.2212].

[43] J. Brod and E. Stamou, *Electric dipole moment constraints on CP-violating heavy-quark Yukawas at next-to-leading order*, *JHEP* **07** (2021) 080, [1810.12303].

[44] J. Brod, Z. Polonsky and E. Stamou, *A precise electron EDM constraint on CP-odd heavy-quark Yukawas*, *JHEP* **06** (2024) 091, [2306.12478].

[45] J. Kumar and E. Mereghetti, *Electric dipole moments in 5+3 flavor weak effective theory*, *JHEP* **09** (2024) 028, [2404.00516].

[46] C.-Y. Seng, *Reexamination of The Standard Model Nucleon Electric Dipole Moment*, *Phys. Rev. C* **91** (2015) 025502, [1411.1476].

[47] Y. Yamaguchi and N. Yamanaka, *Large long-distance contributions to the electric dipole moments of charged leptons in the standard model*, *Phys. Rev. Lett.* **125** (2020) 241802, [2003.08195].

[48] Y. Ema, T. Gao and M. Pospelov, *Standard Model Prediction for Paramagnetic Electric Dipole Moments*, *Phys. Rev. Lett.* **129** (2022) 231801, [2202.10524].

[49] S. Weinberg, *Larger Higgs Exchange Terms in the Neutron Electric Dipole Moment*, *Phys. Rev. Lett.* **63** (1989) 2333.

[50] D. A. Dicus, *Neutron Electric Dipole Moment From Charged Higgs Exchange*, *Phys. Rev.* **D41** (1990) 999.

[51] S. M. Barr and A. Zee, *Electric Dipole Moment of the Electron and of the Neutron*, *Phys. Rev. Lett.* **65** (1990) 21–24.

[52] J. Brod, U. Haisch and J. Zupan, *Constraints on CP-violating Higgs couplings to the third generation*, *JHEP* **11** (2013) 180, [1310.1385].

[53] A. Y. Morozov, *Matrix of mixing of scalar and vector mesons of dimension $D \leq 8$ in QCD. (In Russian)*, *Sov. J. Nucl. Phys.* **40** (1984) 505.

[54] F. Bishara, J. Brod, B. Grinstein and J. Zupan, *Renormalization Group Effects in Dark Matter Interactions*, *JHEP* **03** (2020) 089, [1809.03506].

[55] J. Brod, L. Hüdepohl, E. Stamou and T. Steudtner, *MaRTIn – Manual for the "Massive Recursive Tensor Integration"*, *Comput. Phys. Commun.* **306** (2025) 109372, [2401.04033].

[56] J. A. M. Vermaseren, *New features of FORM*, math-ph/0010025.

[57] A. I. Davydychev and J. Tausk, *Two loop selfenergy diagrams with different masses and the momentum expansion*, *Nucl.Phys.* **B397** (1993) 123–142.

[58] C. Bobeth, M. Misiak and J. Urban, *Photonic penguins at two loops and m_t dependence of BR[$B \to X_s \ell^+ \ell^-$]*, *Nucl.Phys.* **B574** (2000) 291–330, [hep-ph/9910220].

[59] P. Nogueira, *Automatic Feynman graph generation*, *J. Comput. Phys.* **105** (1993) 279–289.

[60] D. Binosi and L. Theussl, *JaxoDraw: A Graphical user interface for drawing Feynman diagrams*, *Comput. Phys. Commun.* **161** (2004) 76–86, [hep-ph/0309015].

[61] J. A. M. Vermaseren, *Axodraw*, *Comput. Phys. Commun.* **83** (1994) 45–58.

[62] J. Brod and M. Gorbahn, *The Z Penguin in Generic Extensions of the Standard Model*, *JHEP* **09** (2019) 027, [1903.05116].

[63] G. 't Hooft and M. J. G. Veltman, *Regularization and Renormalization of Gauge Fields*, *Nucl. Phys.* **B44** (1972) 189–213.

[64] P. Breitenlohner and D. Maison, *Dimensional Renormalization and the Action Principle*, *Commun. Math. Phys.* **52** (1977) 11–38.

[65] J. C. Collins, *Renormalization*, vol. 26 of *Cambridge Monographs on Mathematical Physics*. Cambridge University Press, Cambridge, 1986, 10.1017/CBO9780511622656.

[66] J. Brod, J. M. Cornell, D. Skodras and E. Stamou, *Global constraints on Yukawa operators in the standard model effective theory*, *JHEP* **08** (2022) 294, [2203.03736].

[67] T. Huber, E. Lunghi, M. Misiak and D. Wyler, *Electromagnetic logarithms in $\bar{B} \to X_s l^+ l^-$*, *Nucl. Phys. B* **740** (2006) 105–137, [hep-ph/0512066].